INTERNATIONAL ATOMIC ENERGY AGENCY
UNITED NATIONS EDUCATIONAL, SCIENTIFIC AND CULTURAL ORGANIZATION

INTERNATIONAL CENTRE FOR THEORETICAL PHYSICS
34100 TRIESTE (ITALY) - P.O.B. 586 - MIRAMARE - STRADA COSTIERA 11 - TELEPHONE: 2240-1
CABLE: CENTRATOM - TELEX 460392-1

SMR/388 - 32

SPRING COLLEGE IN MATERIALS SCIENCE
ON
'CERAMICS AND COMPOSITE MATERIALS'
(17 April - 26 May 1989)

SIMULATION OF PERFORMANCE OF NON-HOMOGENEOUS MATERIALS

(Lecture II + Background Material)

E.J. SAVINO
Comision Nacional de Energia Atomica
Departamento de Materiales
Avda del Libertador 8250
Ra-1429
Buenos Aires
Argentina

Review of Elementary Principles

Plasticity in a continuum ideal plastic

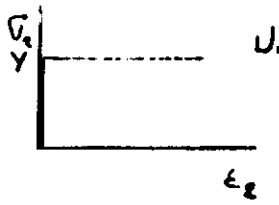

Uniaxial test

at 3dim. stress state ?!
strain ??

In general $\sigma_{ij} = {}'\sigma_{ij} + P\,\delta_{ij}$

Where $P = Tr(\sigma_{ij})/3$ ${}'\underline{\sigma}$: deviatoric stresses

Experimentally it is found flow stress $Y \neq f(P)$

Ideal plasticity $Y = f(\sigma_1 - \sigma_2, \sigma_2 - \sigma_3, \sigma_3 - \sigma_1) = \text{const.}$
where σ_i = i eigenvalue of matrix $\underline{\sigma}$

Different criteria for plastic flow:

Tresca Biggest $(|\sigma_1 - \sigma_2|, |\sigma_2 - \sigma_3|, |\sigma_3 - \sigma_1|) = Y$

Von Misses :
$$(\sigma_1 - \sigma_2)^2 + (\sigma_2 - \sigma_3)^2 + (\sigma_3 - \sigma_1)^2 = 2Y^2 = 3\,{}'\sigma_{ij}\,{}'\sigma_{ij}$$

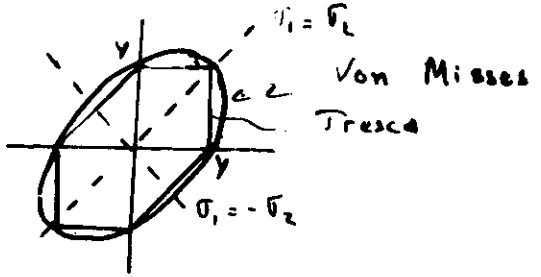

Review of Elementary Principles

Suppose an uniaxial test is performed and the relation between $\underline{\sigma}$ and $\underline{\varepsilon}$ for that test is found. Can one find a general law for any $\underline{\sigma}$, $\underline{\varepsilon}$ state?

Von Misses answer : it exists a pair $(\sigma_e, \varepsilon_e)$ such that, at any state the amount of plastic work:

$$\sigma_{ij}\,d\varepsilon_{ij} = \sigma_e\,d\varepsilon_e \qquad (1)$$

For an incompressible solid, that is where yield does not depend on $Tr(\underline{\sigma})$, it results:

$$\sigma_e = \left(\tfrac{3}{2}\,{}'\sigma_{ij}\,{}'\sigma_{ij}\right)^{1/2} \qquad d\varepsilon_e = \left(\tfrac{2}{3}\,d\varepsilon_{ij}\,d\varepsilon_{ij}\right)$$

How does one compute flow within this classical approach? By using the equation (1) above ⇒ Prandtl-Reuss flow rule:

$$d\varepsilon_i^P = \begin{cases} 3/2\,({}'\sigma_i / \sigma_e)\,d\varepsilon_{ij} & \text{if } \sigma_e = Y \text{ and } d\sigma_e \geq 0 \\ 0 & \text{if } \sigma_e < Y \text{ and } d\sigma_e > 0 \\ & \text{or } \sigma_e = Y \text{ and } d\sigma_e < 0 \end{cases}$$

where Voigt's notation has been used : $i = 1 \to 11$, $i = 2 \to 22$, $i = 3 \to 33$, $4 \to 23$, $5 \to 13$, $6 \to 12$). One can see that the stress / strain states are parallel one to the other.

All the above equations assume ideal plasticity. For small strain cases elastic straining has to be added as done by Prandtl Reuss in their original work and by us when the anisotropic approach is discussed below.

mputer codes generally assume for the strain increments:

$$d\epsilon_{ij}^{T} = d\epsilon_{ij}^{e} + d\epsilon_{ij}^{p} + d\epsilon_{ij}^{\theta}$$

here $\underline{\underline{\epsilon}}^{e}$ = elastic strain (satisfies Hooke law)
$\underline{\underline{\epsilon}}^{p}$ = plastic strain (may satisfy Prandtl-Reuss)
$\underline{\underline{\epsilon}}^{\theta}$ = thermal strain ($= \alpha_i \Delta T \delta_{ij}$, $i = 1,3$)

based on Prandtl Reuss

:veloping an elasto-plastic finite differences code involves large work. However, if the material is isotropic, a reasonable cement with experiments is found, even for very complex ad and/or geometry cases.

le show in the next figures 1 and 2 a grooving notched specimen steel (figure 1) and the predicted stress/strain state compared ith the experimental one, where the stress is measured at the mallest section of the specimen and the strain is taken the ratio: Notch opening displacement / Notch length.

t can be seen that isotropic elasticity, if properly included nto the code, does not do a bad job.

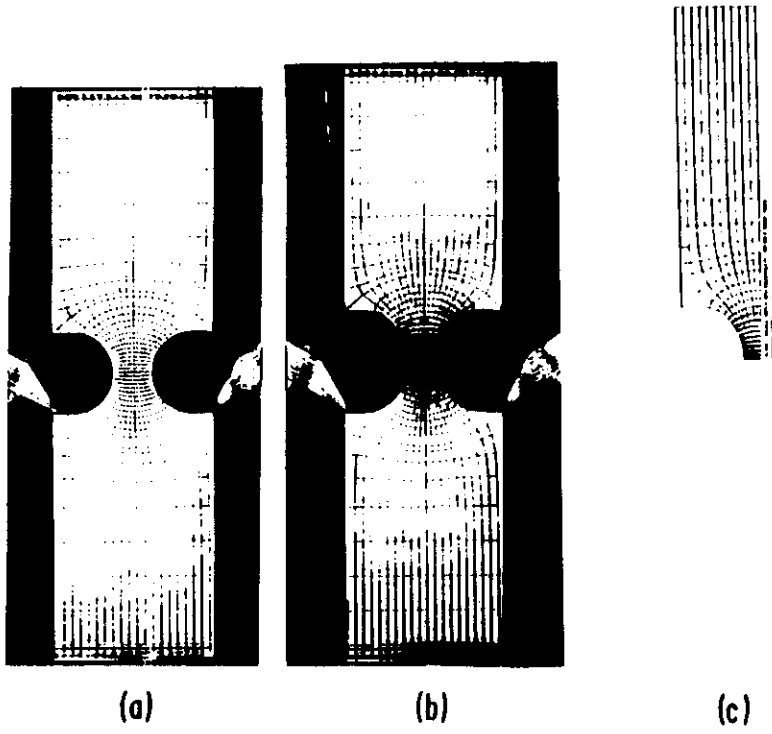

Comparison of Experimental and Calculated Finite Element Mesh: (a) Undeformed, Actual Test Specimen; (b) Deformed to σ_{ave} = 84, 500 psi (580 MPa); and (c) Calculated Mesh after the Deformation. 304 stainless steel deformed at 25°C.

Figure 1 : from EPRI NP-500 RP 456-2, 1977
Plasticity theory and structural analysis of anisotropic metals: Zircaloys

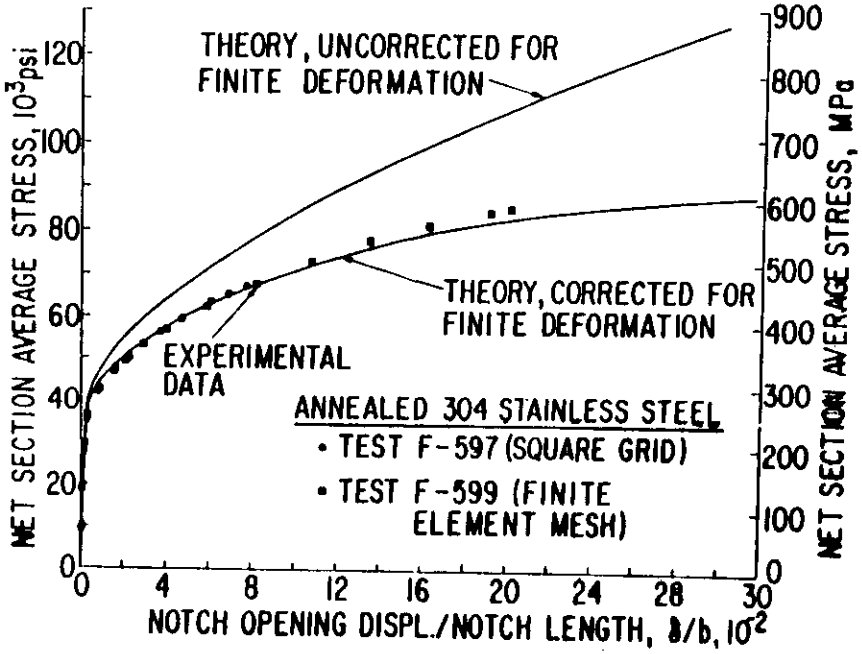

Comparison of Theory with Experiment for 304 Stainless Steel Tested at Room Temperature Under the Plane Stress Loading Condition, (Method A1 - C2)

Figure 2: Same ref. as Fig. 1

L However, even for the mild anisotropy of Cu in a simple test

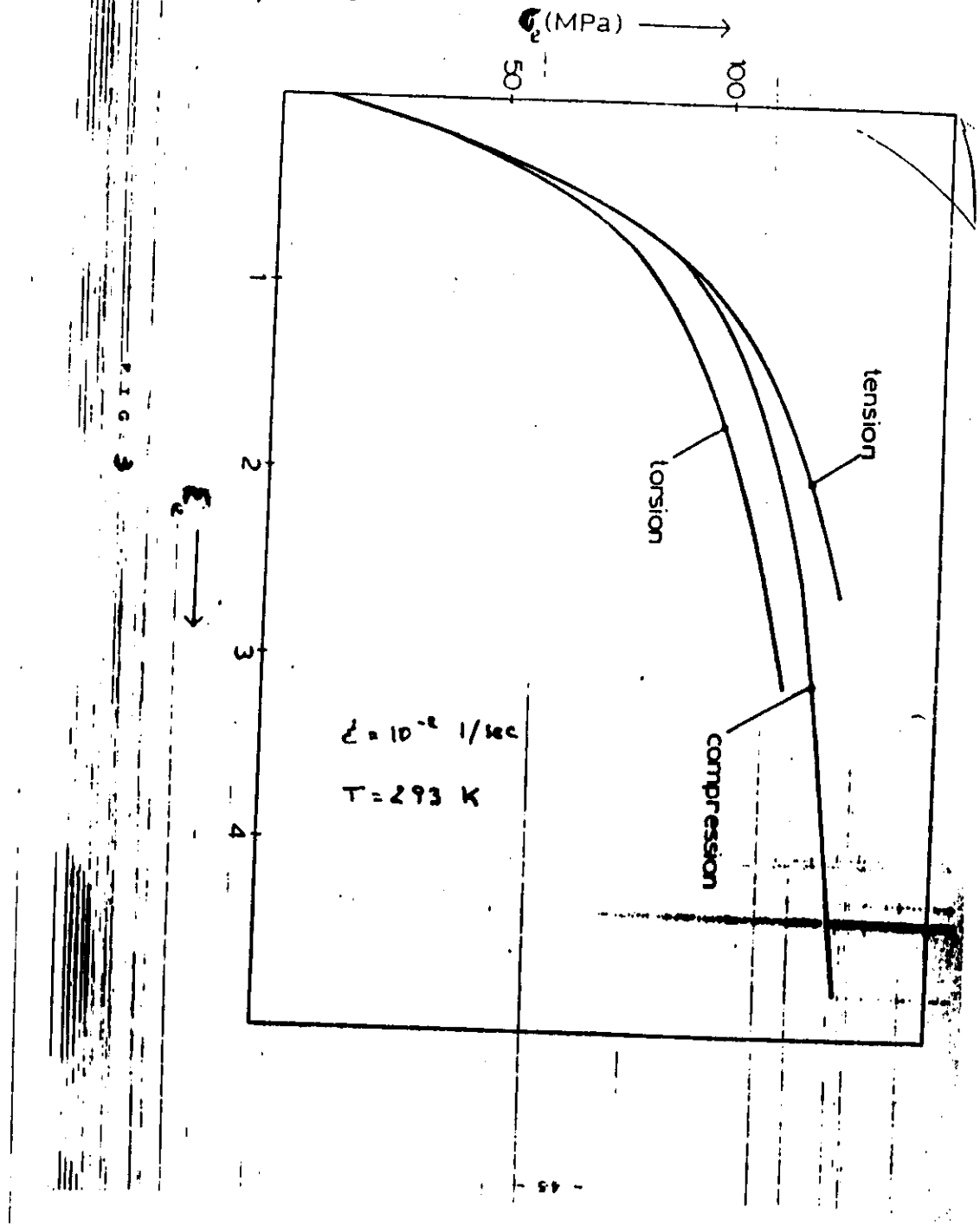

For strongly anisotropic materials, like Zry, and complex stress/strain states, anisotropic plasticity must be included in the calculations:

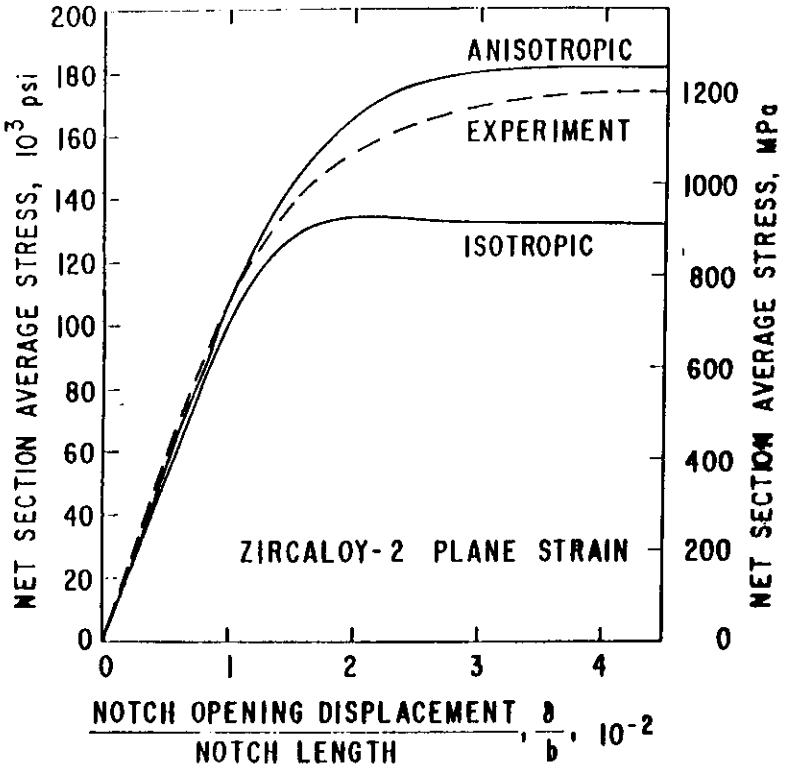

Average Stress Versus Notch Opening Displacement for Zircaloy-2, K-Material, at 25°C. (Method A2-C2)

Fig 4: from same EPRI report as 1 and 2.

17 Continuum approach to anisotropic plasticity

Von Mises yield condition can be writen as a yield function:

$$3f = \tfrac{1}{2}\left[(\sigma_1-\sigma_2)^2+(\sigma_2-\sigma_3)^2+(\sigma_3-\sigma_1)^2\right] - Y^2 = 0$$

and Prandtl Reuss flow rule results

$$d\varepsilon^p_{ij} = \begin{cases} d\lambda\, \partial f/\partial \sigma_{ij} & \text{if } \bar{\sigma}_e = Y \text{ and } d\bar{\sigma}_e > 0 \\ 0 & \text{if } \bar{\sigma}_e < Y \text{ or } d\bar{\sigma}_e \le 0 \end{cases}$$

where $\bar{\sigma}_e = \left(\frac{3}{2}\,'\sigma_{ij}\,'\sigma_{ij}\right)^{1/2}$

and, by employing the isotropic hardening assumption and including elasticity:

$$d\lambda = \frac{1}{2}\left(\frac{1}{E_t}-\frac{1}{E}\right)\frac{d\bar{\sigma}_e}{\bar{\sigma}_e}$$

E = Young's modulus and $E_t = d\bar{\sigma}_e / d\varepsilon^p_e$

For anisotropic yield this approach can be extended into the yield function:

$$3f = M_{ij}\,(\sigma_i-\alpha_i)(\sigma_j-\alpha_j) - Y^2 = 0 \qquad \text{(Voigt's notation is used)}$$

This reduces to Von Misses one for $M_{11}=M_{22}=M_{33}=1$, $M_{12}=M_{23}=M_{31}=-1/2$, $\alpha_1=\alpha_2=\alpha_3=0$

Note that not all M_{ij}, α_i are independent. In case of an incompressible material only 5 are independent parameters.

(For relative importance of anisotropy on technological applications see Harrigan-Savino in background material)

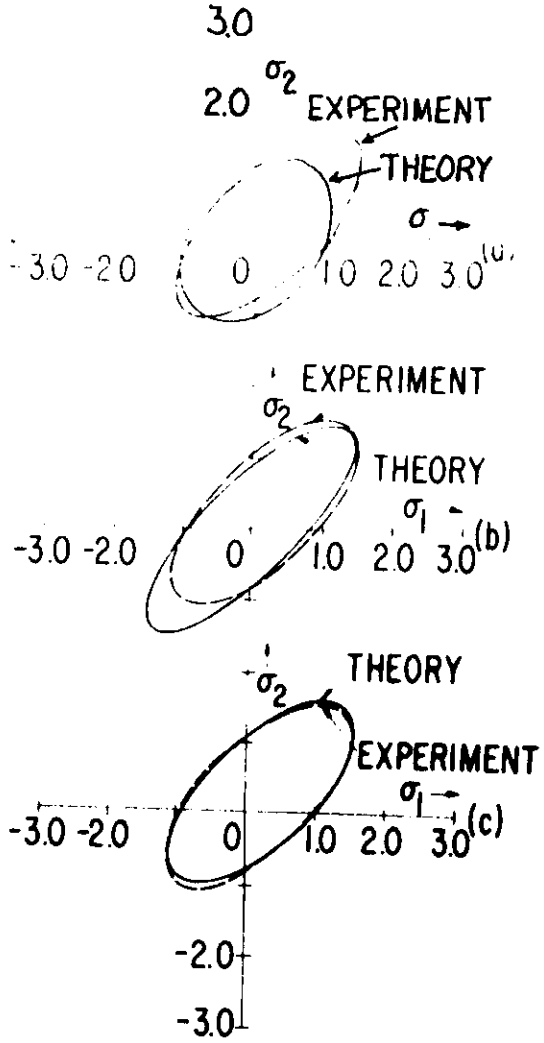

Figure 2.3. Comparison of Theory with Experimental Data: (a) Yield Strengths in Tension Used in Theory; (b) Yield Strengths in Compression Used in Theory; and (c) Yield Strength in Both Tension and Compression Used in Theory.

What is the micro structural reason of macroscopic anisotropic plasticity?

Anisotropic single crystal plasticity

Heterogeneous grain orientation : Texture

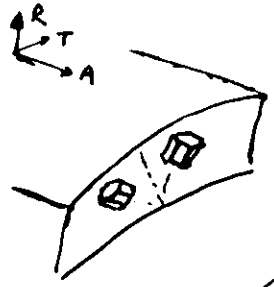

Pole Figure of <0002> direction

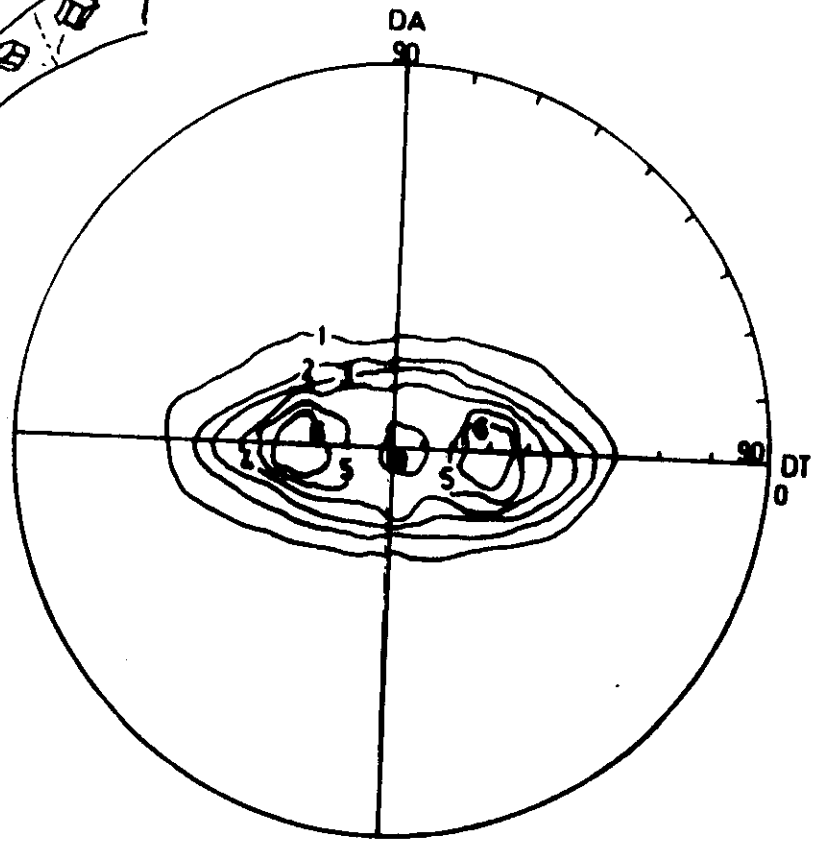

Single crystal

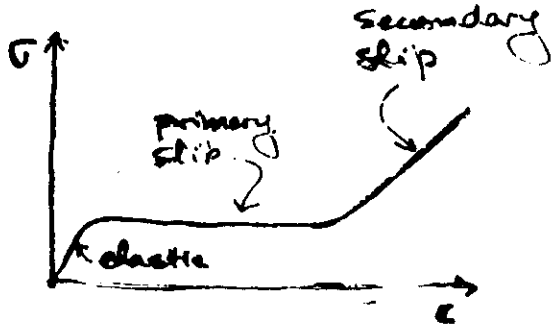

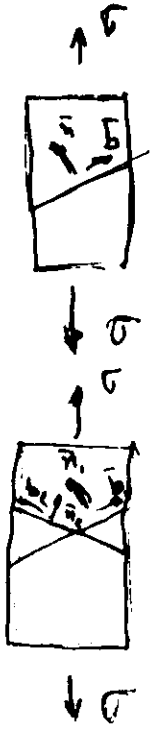

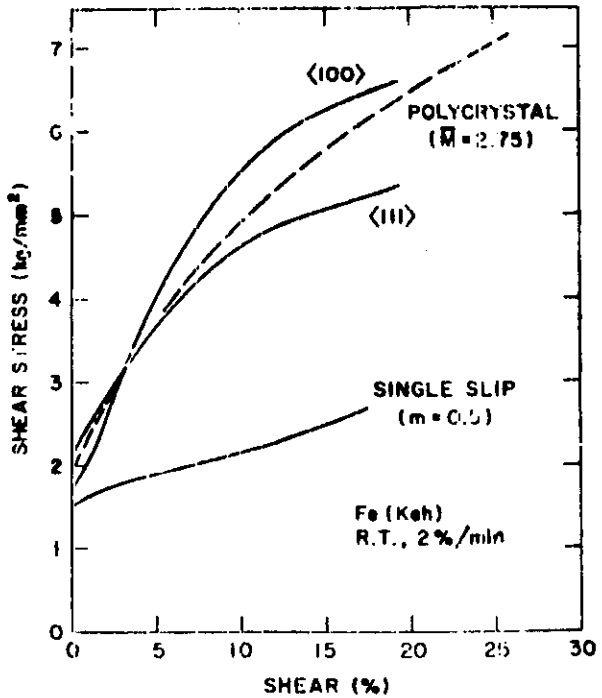

Fig. 17—Shear stress vs shear curves for 99.95 pct Fe (Ferrovac E): three single crystals of controlled orientations and one polycrystal of a grain size of 0.1 mm (15 pct surface grains). After Keh.[75]

Slip systems in fcc

$$\varepsilon_{ij} = \rho \frac{\gamma}{2} (b_i n_j + b_j n_i)$$

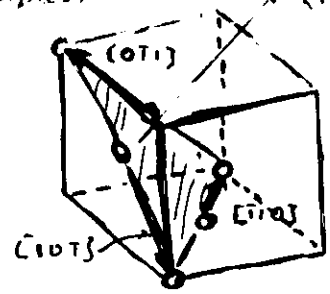

Twinning and slip systems in Zirconium

Twins activated for compresive stresses :

Twin activated for traction stresses :

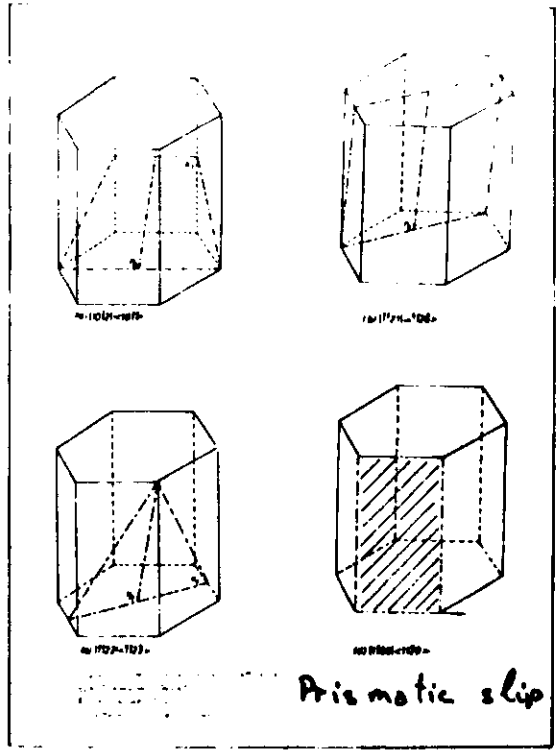

Plasticity of single crystal

$$\gamma = \frac{\partial u'_1}{\partial x'_2} = u'_{12}$$

glide is activated for Critical Resolved Shear Stress τ_c

$$\sigma_\tau = \tau_c = n_i b_j \sigma_{ij} / |b|$$

$$u_{ij} = b_i n_j u'_{12} / |b| = b_i n_j \gamma / |b|$$

Remember $\varepsilon_{ij} = \frac{1}{2}(u_{ij} + u_{ji})$ $\Rightarrow$ in system s

$$\tau_c^{(s)} = m_{ij}^{(s)} \sigma_{ij}$$

$$d\varepsilon_{ij} = m_{ij}^{(s)} d\gamma^{(s)}$$

where $m_{ij}^{(s)} = \frac{1}{2|b|}\left(b_i^{(s)} n_j^{(s)} + b_j^{(s)} n_i^{(s)}\right)$

Plastic work $dw = \sigma_{ij} d\varepsilon_{ij} = \tau_c^{(s)} d\gamma^{(s)}$

As incompressibility is assumed into $b \perp n$ (u_{ij})
$\Rightarrow$
$$dV = d\varepsilon_{11} + d\varepsilon_{22} + d\varepsilon_{33} = 0$$

and remember $\sigma_{ij} = {}'\sigma_{ij} + p\delta_{ij}$

Only the 5 deviatoric stresses are relevant to the problem.

One can work into the space of 5 independent stresses. Define a pseudovector

$$\bar{\sigma} = \left(\frac{{}'\sigma_{11} + {}'\sigma_{22}}{2}, \frac{{}'\sigma_{11} - {}'\sigma_{22}}{2}, \sigma_{23}, \sigma_{13}, \sigma_{12}\right)$$

It results

$$d\bar{\varepsilon} = (d\varepsilon_{11} + d\varepsilon_{22}, d\varepsilon_{11} - d\varepsilon_{22}, 2d\varepsilon_{13}, 2d\varepsilon_{13}, 2d\varepsilon_{12})$$

In a 5 dimension space yield takes place when the pseudovector $\bar{\sigma}$ reaches a plane with normal direction $m \parallel d\varepsilon$ and at a distance $\tau_c^{(s)}$ from the origin.

$$\bar{m} = (m_{11} + m_{22}, m_{11} - m_{22}, 2m_{23}, 2m_{13}, 2m_{12})$$

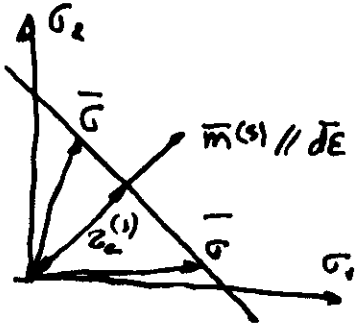

If the stress is fixed as a b.c., it must exist a system of 5 equations (one for each independent component of $d\varepsilon$)

$$\sum_{s=1}^{5} m_k^{(s)} d\gamma^s = d\varepsilon_k \quad (k = 1,5)$$

while the stresses must be at the hyperplane
$\bar{m}^{(s)} \cdot \bar{\sigma}^{(s)} = \tau_c^{(s)}$.

To determine $\sigma^{(s)}$, Bayler postulates:

$$dw = \sum_{s=1}^{5} \tau_c^{(s)} d\gamma^{(s)} = \min \text{ with } \tau_c^{(s)} d\gamma^{(s)} \geq 0$$

Two simple approaches :

Taylor
Keeps compatibility

At each grain g
$\varepsilon^g = \varepsilon^0$

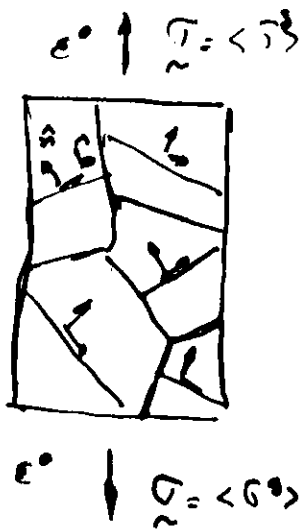

But $\sigma^{g'} \neq \sigma^{g''}$
Non equilibrium

Sachs
Retains equilibrium

$\sigma^g = \sigma^0$

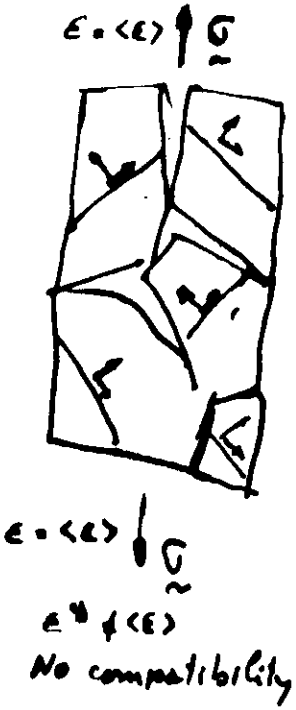

$\varepsilon^g \neq \langle \varepsilon \rangle$
No compatibility

Self consistent model based on Eshelby (1957) !

Kröner, Budiansky, Wu

Each grain isotropic elastic inclusion

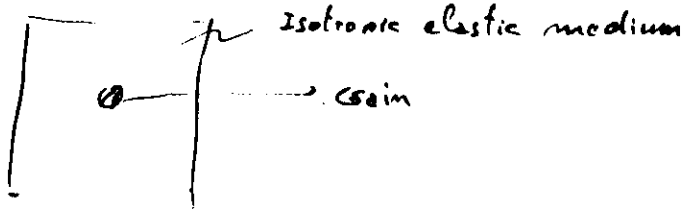

There is the addition of an homogeneous elastic field plus a plastic one.
The source of elastic distortion is the difference between the plastic distortion of each grain and the average one :

$$(\underset{\sim}{\varepsilon}^p_g - \underset{\sim}{\bar{\varepsilon}}^p)$$

The elastic distortion and stresses are average as done at previous lecture for polycrystals but including the grain as source of straining and homogeneous isotropic elastic constants every where.

References in previous lecture notes:
Bishop and Hill, Hutchinson, Kocks, etc.

However remember:

"Real life

Cu „annealed

Tension ($\varepsilon \approx 1$)

compression ($\varepsilon \approx 1.5$)

modelling "real life"

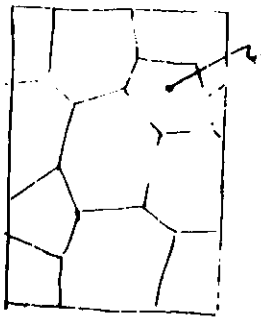

$\underline{G}\, d\underline{\varepsilon}$ homogeneous in each grain

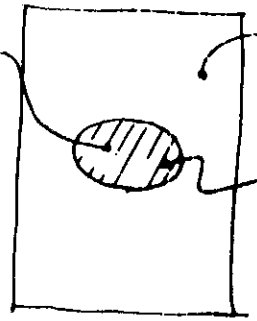

effective medium

Spherical or elliptical grain (inclusion)

Rigid plastic model $\varepsilon \geq 0.5\%$

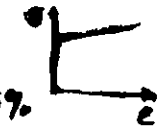

elastic plastic model $\varepsilon \leq 0.5\%$

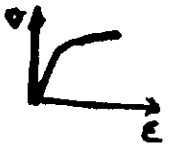

How does a line at the specimen changes when slip at one system takes place?

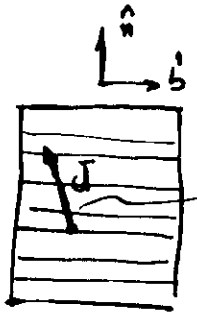

Material line on the surface of the specimen

(this line joins two points of the surface of the specimen)

If $\delta\underline{\varepsilon}$ shear takes place

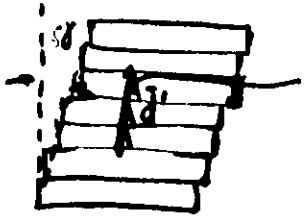

New material line (line joining the same two points)

herefore :

hen only dislocation glide is allowed for at each grain nothing has to be done for keeping boundary conditions.

xample : uniaxial test. Grips must be aligned during l test !

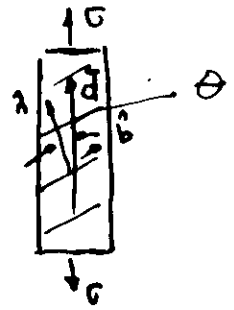

θ : angle between direction of load and normal to slip plane

If only slip in system (n,b) is allowed and one is standing at the crystal system, one sees the stress direction to rotate :

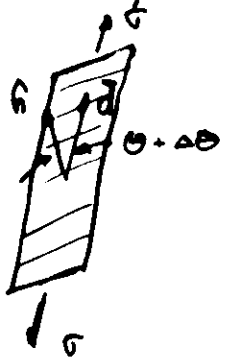

That is from a system at the laboratory :

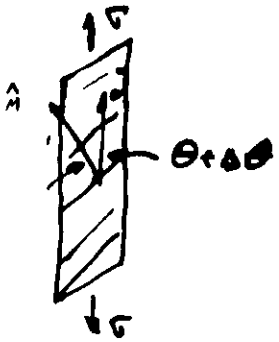

The grain has rotated by an angle $-\Delta\theta$ at the laboratory system.

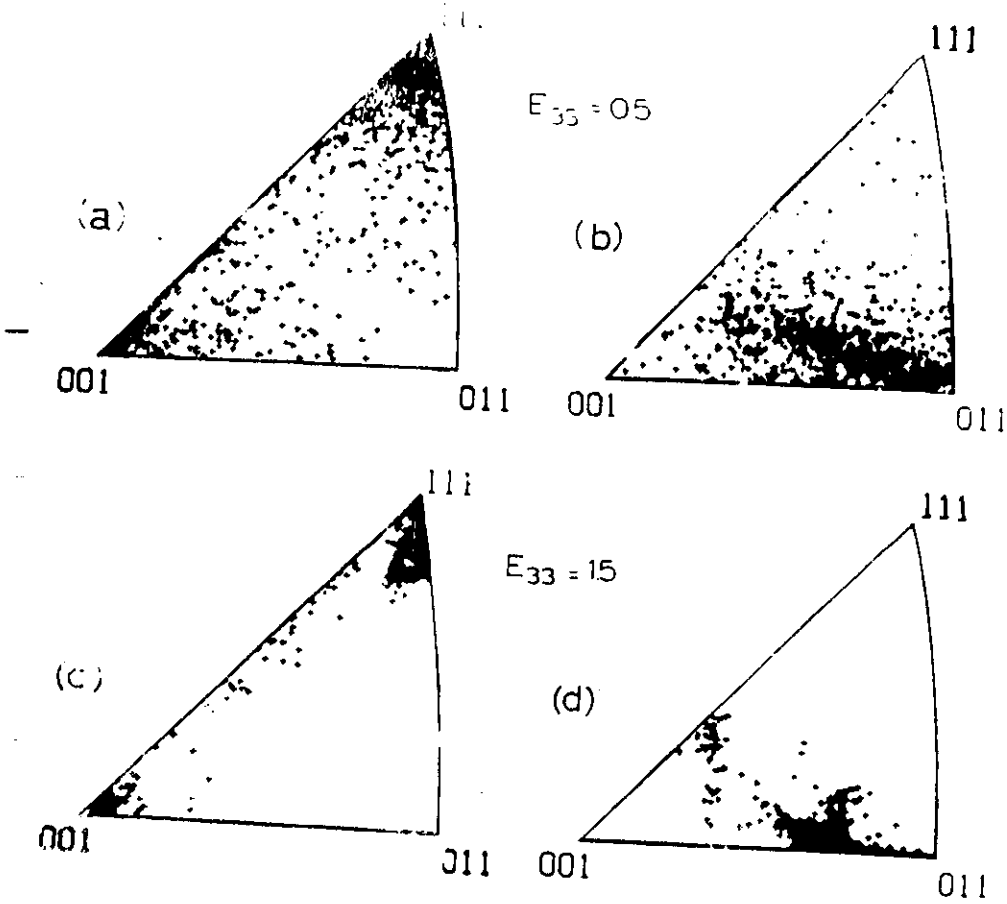

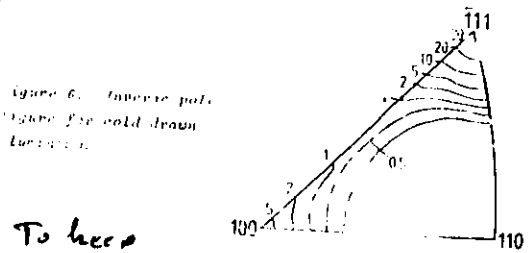

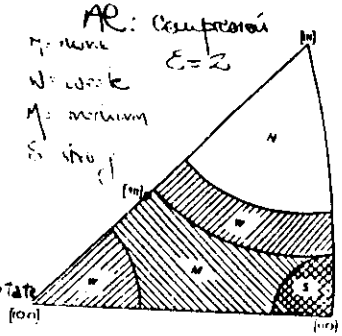

To keep boundary conditions the grains must rotate

Some results for texture evolution due to this rotation

THE BACO (BARRA COMBUSTIBLE) CODE: ITS APPLICATION TO NATURAL URANIUM FUEL RODS

S.Harriague and E.J.Savino
Departamento Materiales
Comisión Nacional de Energía Atómica

ABSTRACT:

The BACO code simulates the thermomechanical behaviour of a cylindrical fuel rod in a power reactor. Its necessary input parameters as well as the output predictions are described, and the appropiate models referred to. The literature reported experiments used for the code calibration are briefly reviewed. Then, results for a self-standing (CNA-1 type) and a collapsable cladding (CNE type) fuel rod are presented. Technologically sound results are obtained, showing that the same numerical code can be used for quite different fuel rods as far as it is based on physically valid, general models, and a numerical stable integration procedure.

1. Introduction -

The code BACO(BArra COmbustible) has been developed at CNEA within a system of codes for fuel modelling.This(1) system includes finite differences methods for simulating the quasi-steady state thermomechanical state of a cylindical fuel rod(BACO), finite elements for calculating local phenomena [2] and recently finite differences methods for transient thermal behaviour and phase change in a cylindrical rod have been incorporated[3,4].

BACO is based in the codes PELT and VAINA developed as a joint exercise with J.Matthews[5] in 1974. The first simulations of a fuel rod section were done by 1976. Since 1977 the code has been: a) extensively described in the international literature[6,7], b) submitted to different convergency tests[7], also c) compared its predictions with analytic solutions in simplified thermomechanical problems[7], while d) new material behaviour models,of different complexity,have been incorporated taking profit of the code modular character[8,9]. On the other side the code predictions have been e) compared with available experimental results for nuclear power reactor fuel elements(i.e.case D in Ref.16) and experimental HWR,LWR and FBR fuel rods[10-12] and f) with predictions by other codes of equivalent complexity like URANUS[13] of the IRT,Darmstadt.

A brief summary of the code input parameters, output results and material performance models is given in the next section,while in section 3 some results for a self-standing (CNA-1 type)and a collapsable cladding(CNE-type) fuel rod are presented.

2. The BACO code -

A summary of the main features of BACO is given in Table I. A more explicit description is given in references(6-13). Table II summarizes the main options of thermomechanical models used in the code for a UO_2 pellet canned in a Zry cladding. Table III gives the main input parameters necessary for the code,in addition a user's manual[37] is available. Finally a list of the code predictions (output) for different rod axial sections at selected time steps is given in Table IV.

TABLE I

MAIN FEATURES OF BACO

-THERMOMECHANICAL DESCRIPTION OF A CYLINDRICAL FUEL ROD
-SIMULATES EITHER A SINGLE ROD SECTION OR A COMPLETE ROD INCLUDING AXIAL FORCES.
-THERMAL DESCRIPTION: QUASI STEADY STATE BASED ON SIMULTANEOUS ANALYTIC AND FINITE DIFFERENCES METHOD[14].
-MECHANICAL DESCRIPTION: FINITE DIFFERENCES METHOD, QUASI-BIDIMENSIONAL, MODIFIED PLAIN STRAIN.
-MATERIAL MODELS: MODULAR STRUCTURE.
-WIDE RANGE OF ROD DESIGN APPLICABILITY.
-ACCURATE CONVERGENCE AND FAST RUNNING.

TABLE III

INPUT PARAMETERS

ROD GEOMETRY(COLD ROD):	Fuel inner radius
	Fuel outer radius
	Dishing depth
	Dishing radius
	Number of dishings per pellet
	Pellet height
	Cladding inner radius
	Cladding outer radius
	Rod length
	Plenum volume
BOUNDARY CONDITIONS :	Coolant temperature
	Coolant pressure
	Rod-coolant heat transfer
	Filling gas composition
	Filling gas pressure
	Washers and/or axial spring constant
IRRADIATION CONDITIONS:	Power cycle; LHGR vs time/burn up
	Cladding gamma heating
	Fast neutron flux
	Flux depression
MATERIAL PROPERTIES:	Those referred to in Table II can be freely combined

TABLE II

THERMOMECHANICAL MODELS USED IN BACO

Thermal models:	Fuel thermal conductivity: Refs.(15),(16),(17),(18) or (19)
	Fuel-cladding heat conductance: Ref.(20),(21),(22)or(23)
	Cladding thermal conductivity: Ref.(24) or (17)
	Coolant thermal model: Heat conductance for film transfer
	Flux depression: Bessel function radial dependence or parabolic radial dependence
	Cladding gamma heating: optional input
Fuel mechanics:	Elastic constants: Ref.(16),(17) or (25)
	Thermal expansion: Ref.(16),(17) or (26)
	Creep: Ref.(16) or (25)
	Restructuring: Ref.(16)
	Densification: Ref.(27) or empirical exponential dependence on burn up
	Cracking: Ref.(16) or (25)
	Swelling: Ref.(16) or (28)
	Change in geometry: Dishing evolution: Generalized plain strain, or a continuum approx.
	Central fuel hole; continuum approx.
	Grain growth: Ref.(17)
Cladding mechanics:	(Zry-S.Steel)(Zry models are given-Anisotropic mech)
	Elastic constants: Ref.(16),(29) or (30)
	Tube texture: Ref.(31) or experimental values
	Thermal expansion: Ref.(24) or (32)
	Time independent plasticity: Ref.(29)
	Creep: Ref.(16),(32) or (33)
	Radiation growth: Ref.(32) or (34)
Fission gas release:	Ref.(16),(35) or (36)

TABLE IV

BACO'S PREDICTIONS(OUTPUT) AT SELECTED TIME STEPS

Thermal predictions: Pellet, cladding and coolant temperature profile

Neutronic calculations: Flux depression
Fast flux at cladding

Mechanical predictions: Fuel and cladding radial deformation, including central hole at fuel
Fuel and cladding stress/strain state
Fuel cracking(radial and axial), including central hole opening or closing down and crack volume
Fuel-cladding contact pressure
Dishing profile
Cladding ridging
Fuel and cladding axial strain

Material state predictions:
Fuel density vs.radius
Fuel grain size radial dependence
Fuel fission gas storage
Cladding internal stresses

Synergetic predictions: Internal gas pressure and composition (fission gas release per radial and axial section)
Rod axial stress/strain

3. HWR fuel rod simulation -

Some numerical results for a self standing (CNA-1 type) and collapsable(CNE type) cladding fuel rod are presented. The first corresponds to a set of design parameters similar to those of an Atucha-I fuel rod, while the second is correlated to an Embalse rod. Hypothetical typical irradiation conditions are assumed and the effects of a general power increase are analysed.

The assumed power cycle of the CNA-I rod is sketched in figure 1(where only power at the highest power axial position is shown): the cycle includes two changes in the position of the fuel bundle within the reactor at 76 and 116 fpd, and power

peaks due to local changes, i.e. control rod motion, changes in near fuel bundles, etc.. In the two changes(76 and 116 fpd) the fuel goes through a zero power, reactor conditions state, while the EOL results are calculated at stp conditions. Fuel predicted central temperature at the highest power axial section is also plotted in figure 1 for the power cycle shown(100%) and for a 15% general power increase (115%). As expected temperature and power closely correlate, except for the decrease in central temperature at constant power for the first 10 days of irradiation. This is due to fuel-cladding gap closing down induced by a large primary creep of the cladding.

It can be seen in figure 2 that for the material models used in the calculation both the cladding and pellet radius decrease during that initial period. In the case of the pellet this is due to redensification; however cladding creep down dominates and the final result is a reduction in hot gap width. For the 100% case, pellet-clad contact is stablished at 44fpd and gap reopens at the third bundle position; while for the high power case(115%) gap closes at 8fpd and does not reopen during the whole cycle. Predicted contact pressures are plotted in figure 3, also for the high power axial section and for the 100% and 115% cases.

The amount of fission gas release by using the Beyer and Hann model[16,35] is plotted in figure 4. It can be seen a relatively small increase in power(15%) gives a 100% increase in gas release. However, due to the relatively large initial He content(the rod is pre-pressurised) the fraction of fission gas is relatively low and gap conductance large during both cycles. A central hole opening by restructuring is predicted for the 115% case at the second position in the reactor, while ridging is predicted for both cases.

The power cycles for simulating a CNE type rod performance are summarized in figure 5(standard power) and 6 (high power) together with the predicted fuel central temperature. Power axial profile is not important here for a short rod (50 cm) against the above CNA-1 type case for a long bundle (app.6 m). In figure 6 the results for two different gas release models -(35,16) against (36)- are reported. In figure 7 the predicted amount of fission gas release is plotted. Fission gas release has a larger influence for the CNE rod performance than for the CNA-1, this is due to the different initial amount of He content which is 20 times larger for the

CNA-1 than here. Also the relative free inner volume is smaller here than for the CNA-1,and rod power at the high power position is almost axially independent. These facts imply a higher fission gas poisoning into the fuel-clad conductance and,therefore,a large influence of gas release in fuel temperature (figure 6). Then,for the high power case,a central hole opening by restructuring is predicted for either gas release models. The hole radius is plotted in figure 8;it is a small hole but its influence in the fuel stress/strain state is relevant. Contact pressure is plotted for the two power cycles in figures 9 and 10. In spite larger central temperatures are predicted for the high power case,the contact pressure is relaxed in that case by closing the central hole. The general shape of the contact pressure curves responds to a large initial value,due to differential thermo-elastic expansion,which is relaxed after the first days of irradiation by cladding primary creep,fuel redensification,restructuring and central hole closing down (these last two for the high power case). Fuel swelling dominates contact pressure increase after that initial relaxation.

Gas pressure,which is assumed to be the same at any interstice within the rod including central hole,is plotted in figure 11,where also the coolant pressure is shown. It can be seen that for the high power-high gas release case a situation is reached where internal pressure at the central hole is larger than coolant pressure over the external surface of the cladding. As a result the central hole closing down stops and contact pressure relaxation rate decreases. Axial strains are also shown in figures 8 and 9.

4. Summary -

The BACO code has been shortly described and applied to the two types of fuel rods used in the argentine power reactors. A brief power and model sensitivity analysis was tried. The previous results should then be taken within that spirit. The comparative predictive performance of the two rods and of the same rod under different power and/or with different material models discussed in section 3,are technologically feasible,physically understandable and ellucidating for design decisions.

Acknowledgement: We acknowledge support from the Departamento Combustibles Nucleares,CNEA.

References:

1- S.Harriague,E.J.Savino,G.Coroli,F.G.Basombrio and G.Sanchez Sarmiento -Nucl.Eng.Des.56 (1980),p.83.
2- F.G.Basombrio and G.Sanchez Sarmiento -Nucl.Eng.Des.49 (1978), p.231. Also same authors in Res Mechan.1 (1979).
3- C.A.Baigorria,S.Harriague and E.J.Savino -Proceed.SMiRT-7,(1983), C 3/5.
4- C.A.Baigorria -Proceed.1st.LatinAmerican Congress on Heat and Mass Transfer,2 (1982),p.1119.
5- S.Harriague,J.R.Matthews and E.J.Savino -AERE-M 2916 (1977).
6- S.Harriague,G.Coroli and E.J.Savino -Proceed.SMiRT-5 (1979),D 1/2.
7- S.Harriague,G.Coroli and E.J.Savino -Nucl.Eng.Des.56 (1980),p.91.
8- S.Harriague and E.J.Savino -SMiRT-5 Post Conference Specialists Meeting on Fuel Computer Simulation (1979).
9- S.Harriague,E.J.Savino,C.A.Baigorria and N.S.de De Grande -Proceed. SMiRT-7,(1983),C 1/7.
10-C.A.Baigorria and E.J.Savino -VI Panamerican Conference on Materials Technology,Mexico(1981).
11-E.Forlerer,G.Coroli,S.Harriague,E.J.Savino and H.Elbel -Meeting Asociacion Argentina de Tecnologia Nuclear,S.C.de Bariloche(1980).
12-S.Harriague and E.J.Savino -Internal Report to Ib Misfeldt,Risø National Laboratory (1983).
13-T.Preusser,S.Harriague,E.J.Savino and C.A.Baigorria -CNEA Report (to be published).
14-S.Harriague and H.Elbel -Report PMM/I-250 (1977).
15-M.F.Lyons -GEAP-5100-1 (1966).
16-H.R.Freeburn,S.R.Pati,I.B.Piero and M.G.Andrews -EPRI-NP 369(1977)
17-MATPRO-09 -Tree-NUREG -1005 (1976).
18-R.Brandt and G.Neuer -J.Non-Equil.Therm. 1,(1976),p.3.
19-J.A.Christensen -Halden Report HPR-84 (1974).
20-A.M.Ross and R.L.Stoute -AECL 1552 (1962).
21-K.Lassmann -Wärme und Stoffübertragung 12 (1979),p.185.
22-F.R.Campbell,L.R.Bourque,R.Deshaies,H.Sills and M.Notley -AECL-5400 (1976).

23-J.M.Broughton and P.Mac Donald in MATPRO-09,App.C,TREE-NUREG-1005.
24-D.B.Scott -WCAP-3269-41 (1965).
25-J.R.Matthews -AERE -M 2643 (1974).
26-J.Roth and F.K.Halteman -NUMEC-2389-9 (1965).
27-H.Assmann,G.Maier and H.Stehle -Reaktortagung,Nuremberg (1975).
28-J.H.Gittus in Int.Conf.on Physical Metallurgy of Reactor Fuel Elements,Berkeley Nucl.Labs.(1973).
29-A.Casario and D.Santinelli -CNEA 13/75/D-CN (1975).
30-Nothwood,London and Bahen -J.Nucl.Mat.55(1975),p.299.
31-H.Stehle,E.Steinberg and E.Tenckhoff -ASTM-STP 633,(1977),p.486.
32-E.J.Savino and C.E.Laciana -J.Nucl.Mat.90,(1980),p.89.
33-P.A.Ross-Ross and C.E.L.Hunt -J.Nucl.Mat.26,(1968),p.2.
34-H.Elbel and D.Gobel -KfK-Ext.6/73-4 (1973).
35-C.I.Beyer and C.R.Hann -BNWL-1872 (1974).
36-J.Weisman,P.E.Mac Donald et al.-Trans.ANS,12 (1969),p.900. Constants from ref.17,p.140.
37-BACO User's Manual -(1980).

(4)

C.N.D. FUEL CENTRAL Temperature

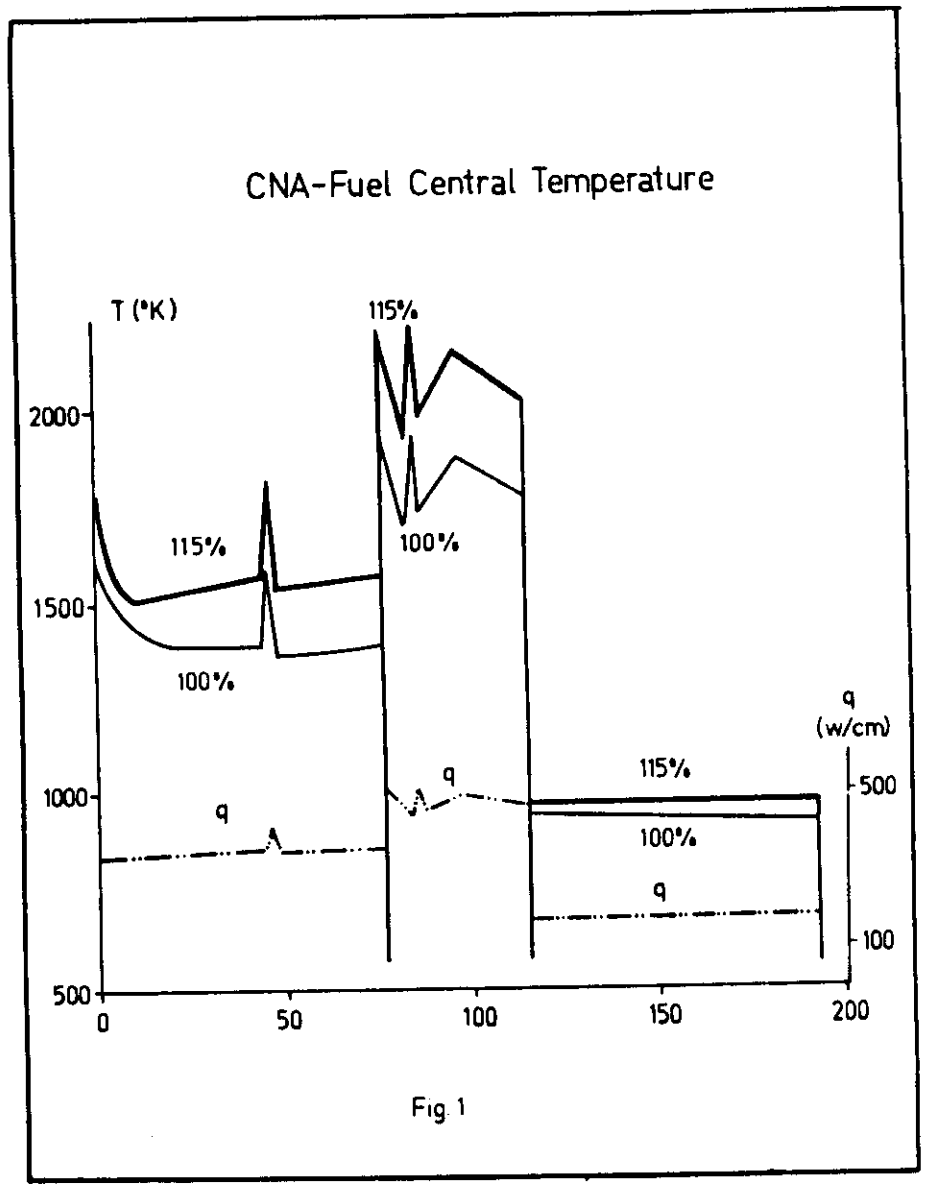

Fig. 1

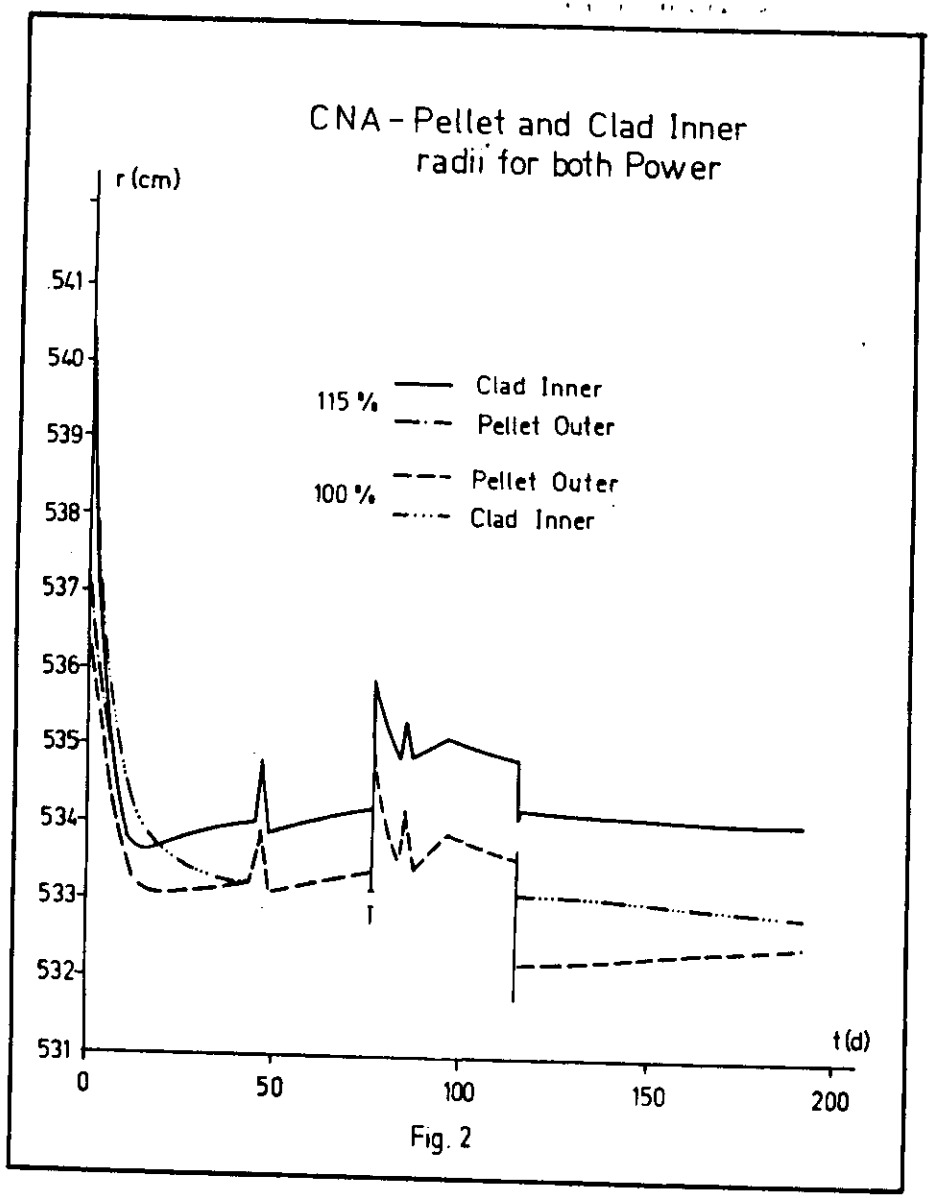
CNA - Pellet and Clad Inner radii for both Power
r (cm)
541
540
539
538
537
536
535
534
533
532
531
115 %
Clad Inner
Pellet Outer
100 %
Pellet Outer
Clad Inner
0
50
100
150
200
t (d)

Fig. 2

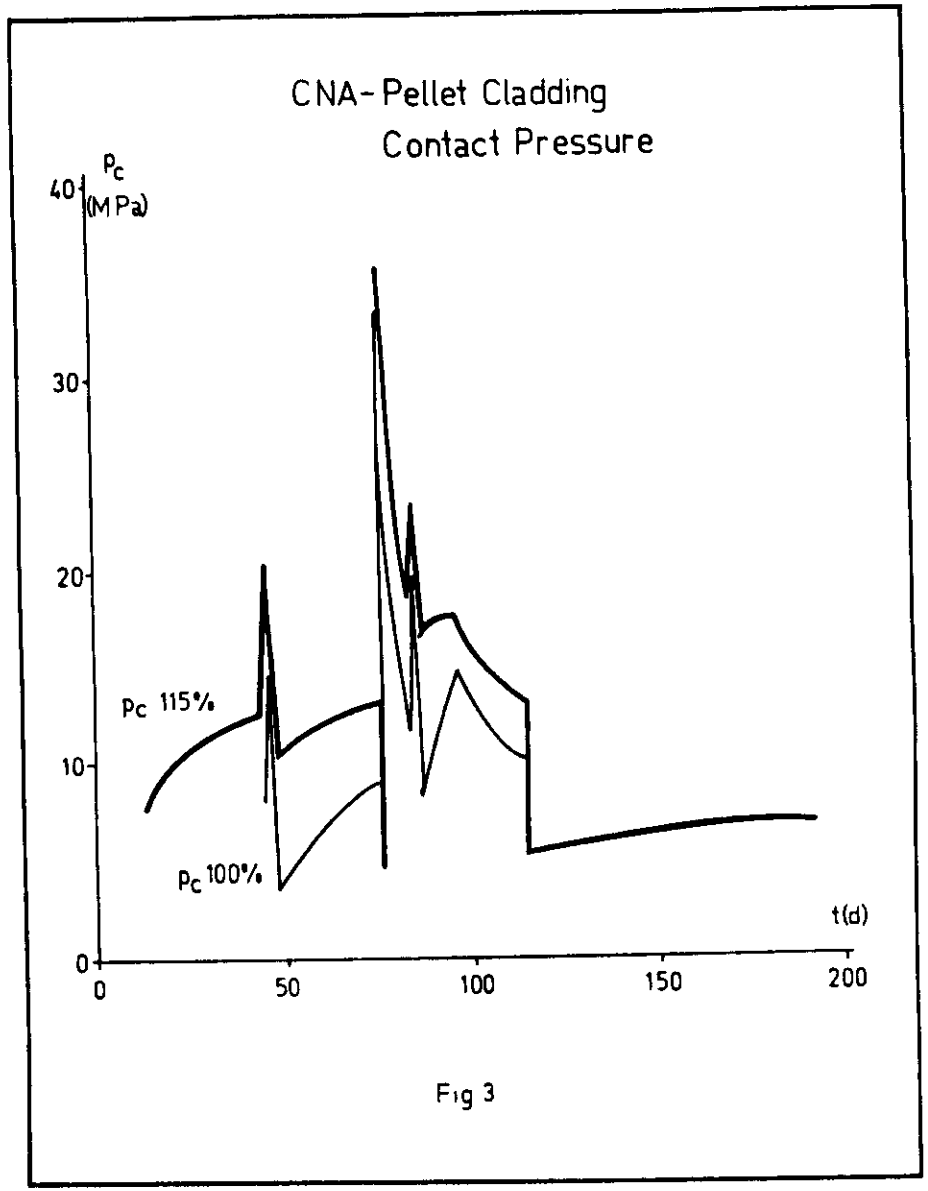
CNA - Pellet Cladding Contact Pressure
Pc (MPa)
40
30
20
10
0
Pc 115%
Pc 100%
0
50
100
150
200
t(d)

Fig 3

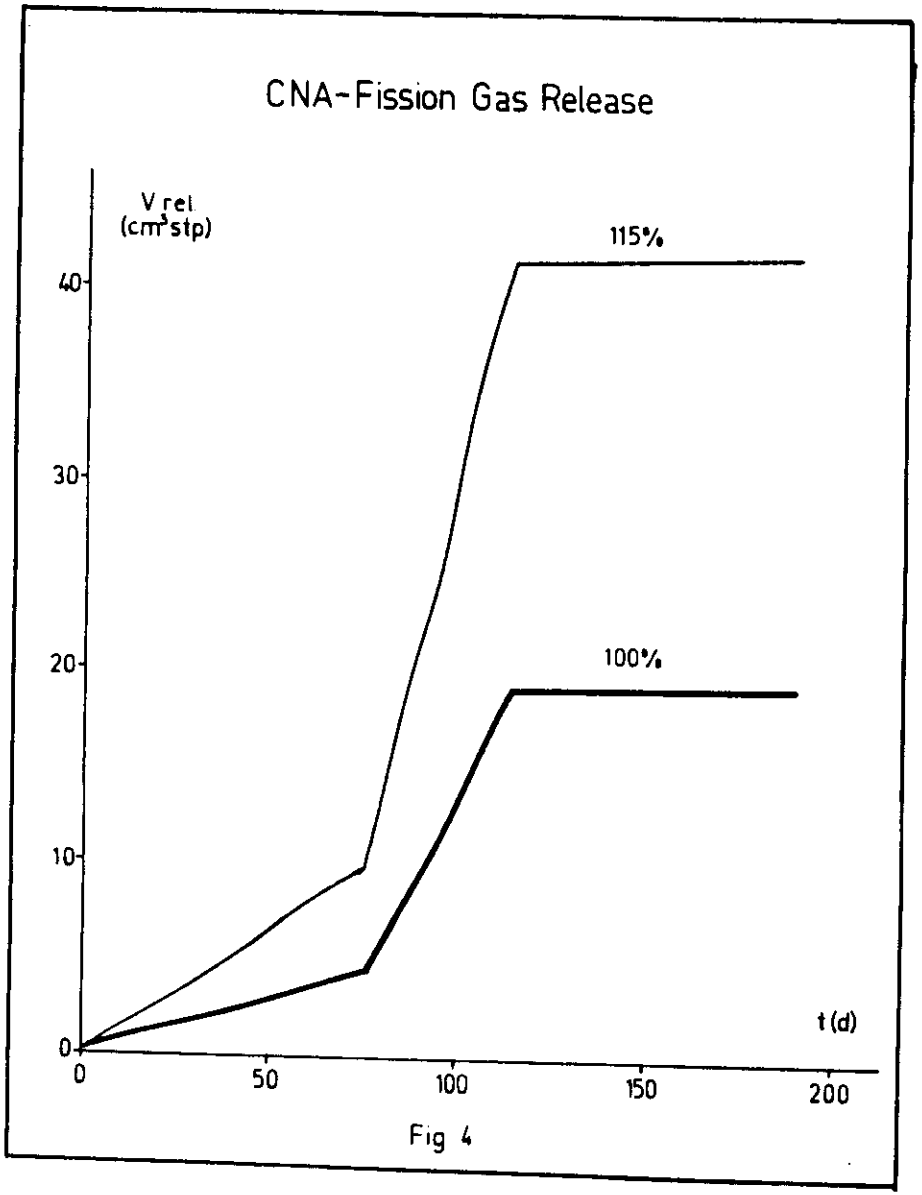
CNA-Fission Gas Release
V rel
(cm³stp)
115%
100%
40
30
20
10
0
t(d)
0
50
100
150
200
Fig 4

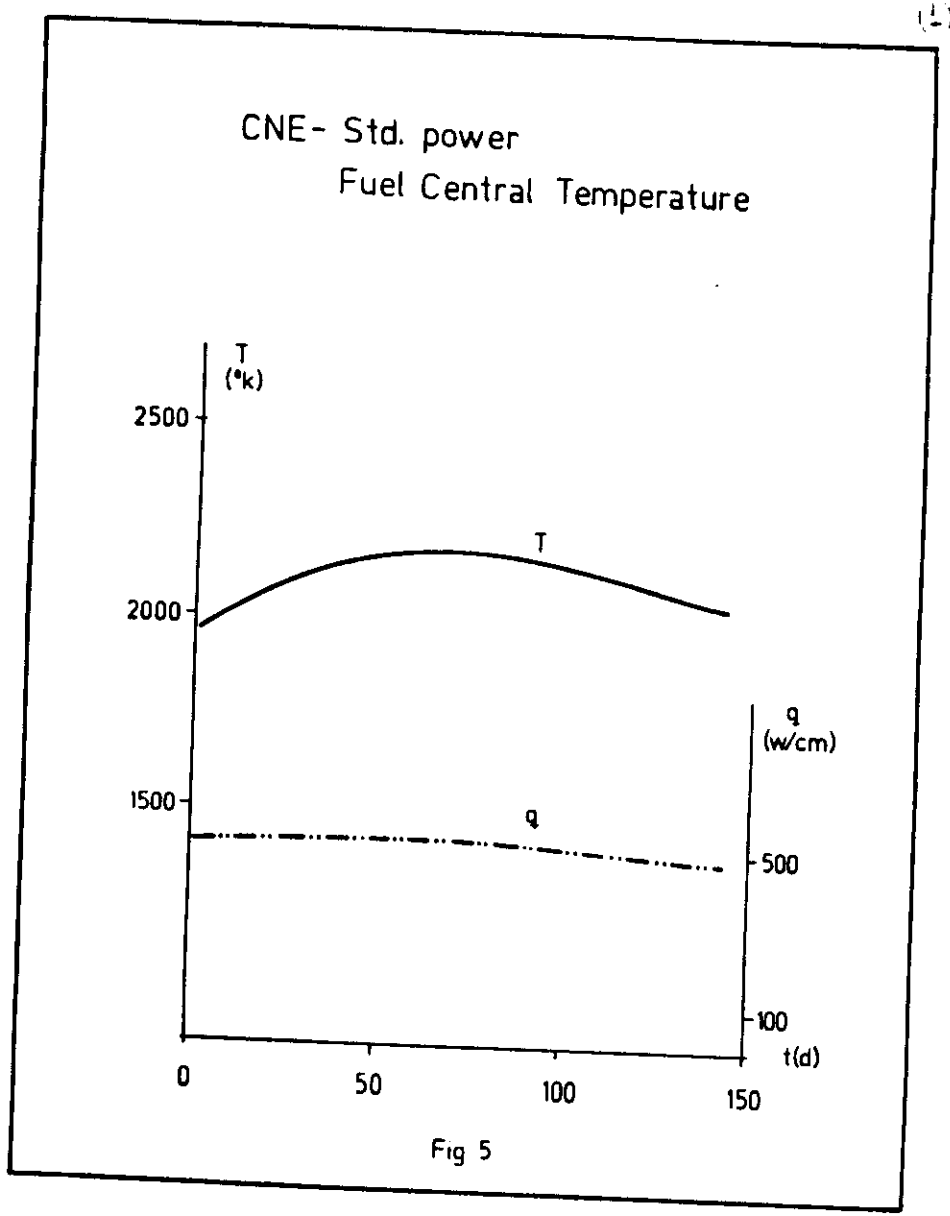
CNE- Std. power
Fuel Central Temperature
T
(°k)
2500
2000
1500
T
q
(w/cm)
500
100
t(d)
0
50
100
150
Fig 5

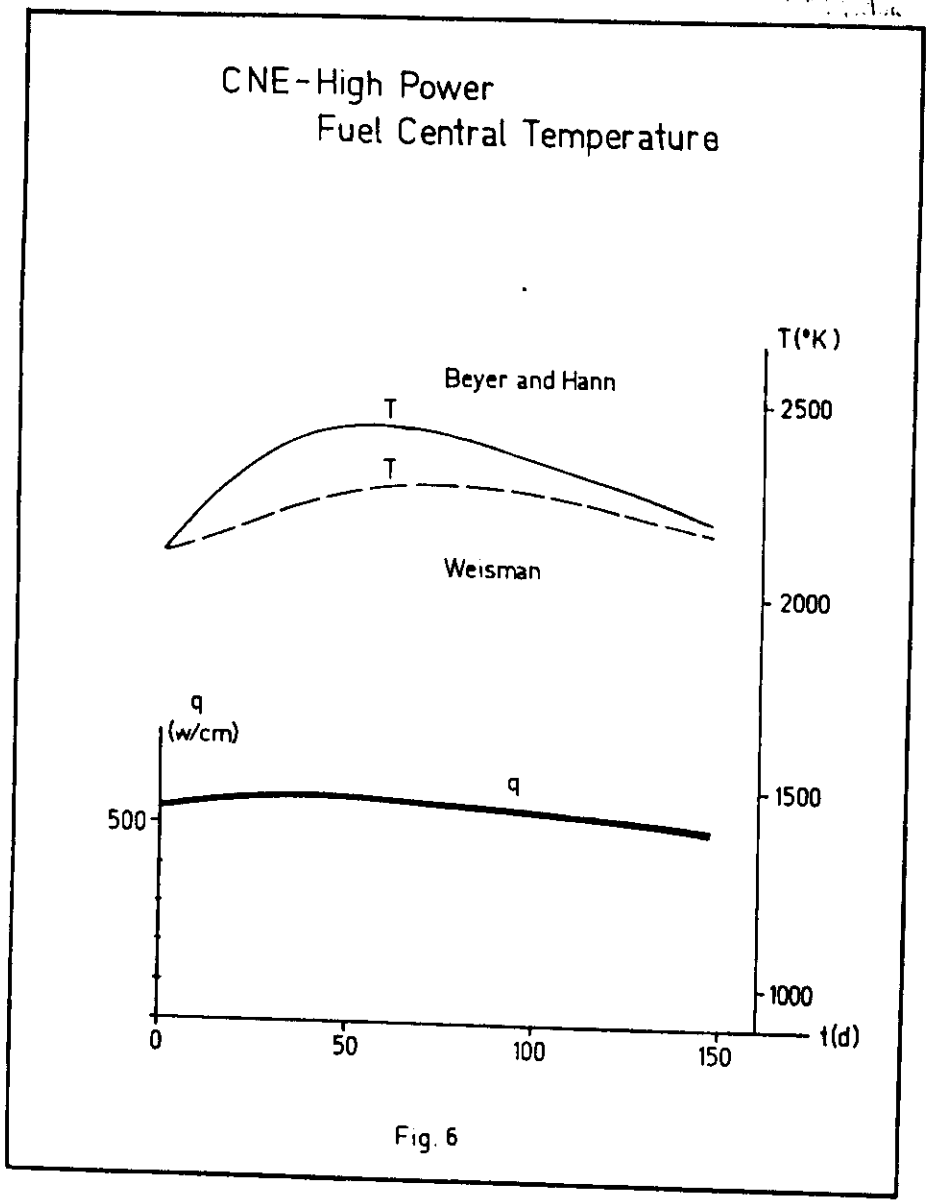
CNE-High Power
Fuel Central Temperature
T(°K)
Beyer and Hann
T
T
2500
2000
Weisman
q
(w/cm)
q
500
1500
1000
0
50
100
150
t(d)

Fig. 6

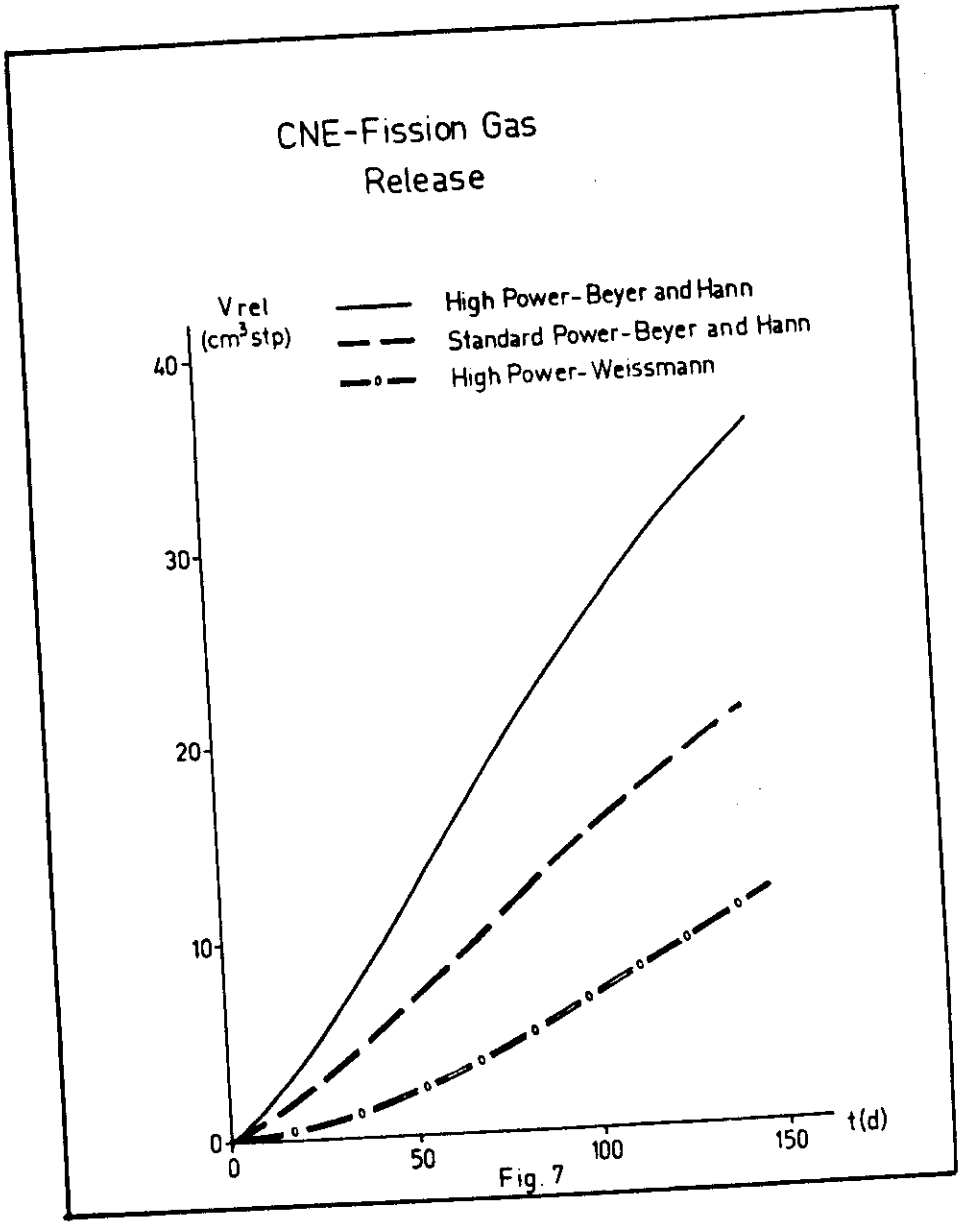
CNE-Fission Gas
Release
Vrel
(cm³stp)
High Power-Beyer and Hann
Standard Power-Beyer and Hann
High Power-Weissmann
40
30
20
10
0
0
50
100
150
t(d)

Fig. 7

CNE- High Power

Central Hole Radius

and Axial Strains

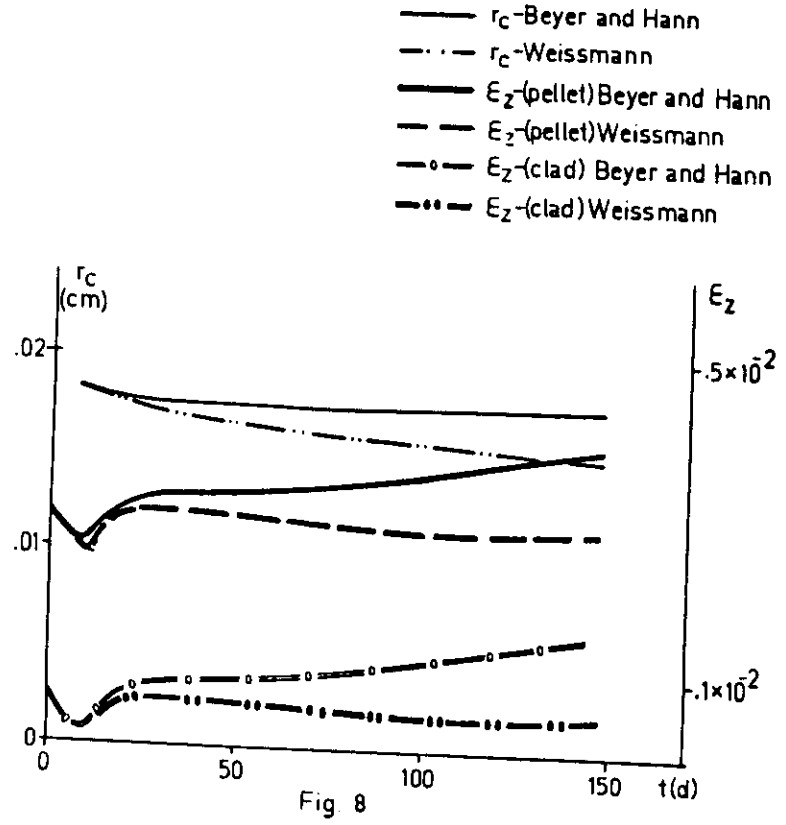

Fig. 8

CNE- Standard Power

Rod Axial Strain and

Pellet-Cladding

Contact Pressure

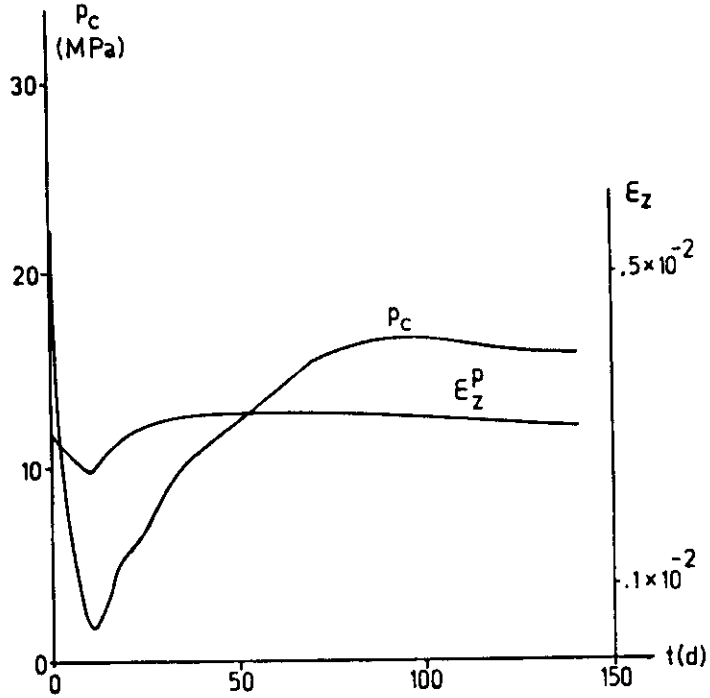

Fig. 9

CNE-High Power
Pellet-Cladding
Contact Pressure

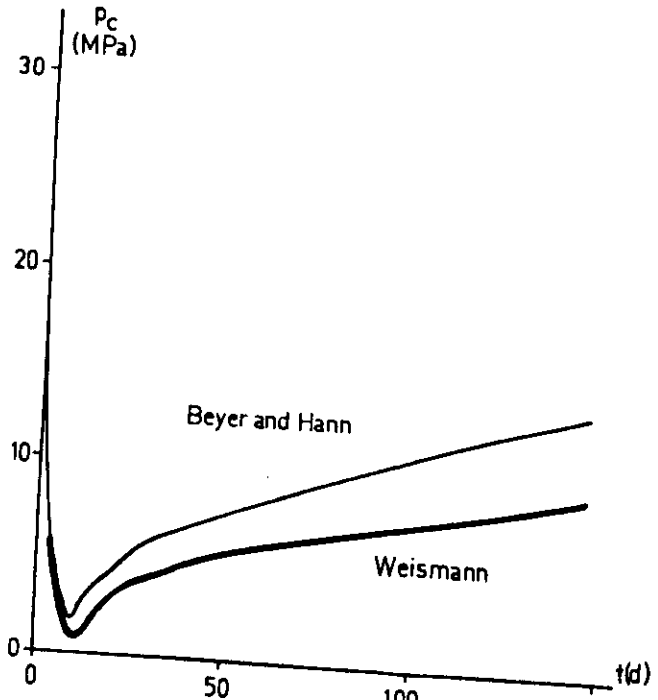

Fig. 10

CNE- Rod Gas Pressure

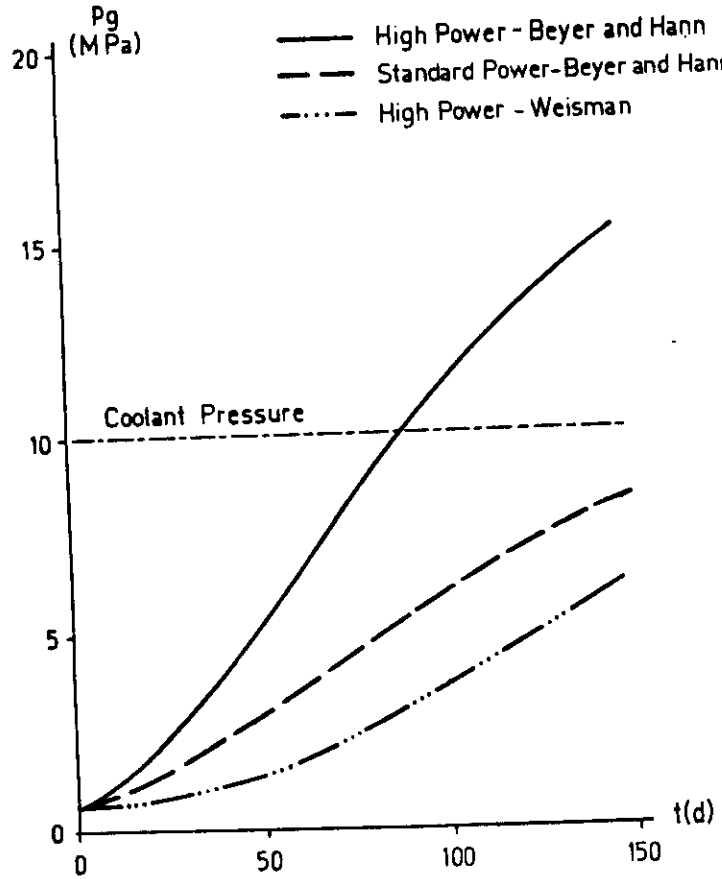

Fig 11

MATERIAL MODELS AND NUMERICAL SIMULATION OF REACTOR FUEL RODS PERFORMANCE

by
S.Harriague and E.J.Savino
Comision Nacional de Energia Atomica
Buenos Aires-Argentina

ABSTRACT -

The influence of different gap conductance parameters, UO_2 and Zry elastic constants and thermal conductivity, and UO_2 fracture stress on the predicted fuel rod performance is studied for a simple power cycle using the BACO code. Significant differences, more than 250°C in predicted fuel central temperature, are obtained using different correlation laws proposed in the literature for UO_2 thermal conductivit The influence of the other above mentioned parameters is less marked for that cycle.

A study is also made of the influence of Zry texture on the fuel rod performance, via the anisotropy coefficients in Hill's model. Claddings having four different annealing textures are simulated; differences of up to 50% are found in the predicted hoop stress at the cladding inner surface, as well as significantly different cladding cre down.

It is concluded on one side that the scattering in different correlations for materials behaviour may have a significant influence on the predicted fuel rod performance. On the other, it is shown that fuel performance may depend strongly on the cladding fabrication thermal treatment, due to the resulting change in texture.

coefficients on the code stress-strain predictions is studied. The purpose of this study is twofold, on one side a model sensitivity determination, on the other an assesment on the influence of the cladding fabrication process parameters on the fuel performance.

2- USE OF DIFFERENT CORRELATION LAWS FOR SOME MATERIAL PROPERTIES

For the numerical examples in this section a simple power cycle is assumed; this is composed of a ramp from zero up to 550 w/cm and a stay at this constant power until a final burnup of 5000 Mw.d/t(U) is reached. Some relevant characteristics of the fuel rod used for the calculation are summarized in Table I.

The BACO code calculates the thermo-elasto-plastic performance of the rod through the numerical integration scheme described by Harriague et al. [2] [3] . The phenomena of thermal expansion, elasto-plastic straining (including work hardening), creep, swelling, redensification , fuel reestructuring and radiation growth are included in the mechanical modeling. Two different cold rod geometries are considered (see Table I) and a set of material models, summarized in Table II of [3] is taken as reference case. Some of these models are changed, one at a time, with the others kept fixed. Some of the predictions of the code which result by adopting this procedure for the cycle above mentioned are summarized in Tables II and III. In the Appendix the material laws which are varied for the different calculations are briefly described.

For Table II (example 1) five variations of the laws in the reference case are made. In cases 1 and 2, the constant $\underline{c}$ in Ross-Stoute law for the gap conductance -see appendix- is varied. It takes the value 2,5 in the reference case; 1.8 in case 1 and 1. in case 2. It can be seen that differences of 50°C in the fuel central temperature are predicted by varying the value of that constant within the above mentioned range.

In cases 3 and 4 the elastic constants of the Zry cladding and UO_2 pellet are changed from those measured at CNCA {11} (which approximately agree with those reported by Northwood et al. {14}) and the ones reported by Matthews {10} ,used in the reference case,to the ones recommended in the EPRI report {6} . From the table it can be concluded that the influence of the elastic response on the reported values is relatively small. Finally,in case 5 the constant value of 150 MPa assumed for the UO_2 fracture stress in the reference case is replaced for the law recommended at {8} - see appendix-. This change has a negligible influence in the reported results,

In the example reported in Table III we concentrate in the thermal conductivity of both UO_2 and Zry. As it is well known, thermal conductivity is a heinous parameter to determine for a ceramic. Several fits have been proposed in the literature for the UO_2 thermal conductivity. One of the first ones is due to Lyions {4} and it is used in our reference case. In Figure 1 we plot it, together with several later correlations, for a 95% TD oxide as a function of temperature. As a general comment it can be seen that Lyons fitting gives the smallest conductivity values.However the largest scattering among the proposed laws takes place at relatively high temperatures (over 2300°C). In Table III some thermomechanical values predicted by the BACO code are reported for the power cycle above descripted. As expected, larger temperatures are predicted when Lyons law is used. At the end of the power up ramp,the central fuel temperatures are ordered in a proportion inverse to the average conductivity value over the whole temperature range (between 480 and 2200°C). By the end of the power cycle this order is slightly altered,i.e.compare the EPRI law with the one due to Christensen; the fact that the calculation using the last law predicts a larger central fuel temperature is due to the different fitting of the conductivity in the low temperature range (between 410 and 510°C). A cooler fuel for the same initial geometry implies later pellet-cladding contact, and therefore lower stresses are predicted at the cladding-see last two columns of the table. Finally,the temperature dependent thermal of the Zry

proposed by EPRI is used in case 6. It can be seen it has a minor influence on the fuel temperature. It is interesting to point out in this example that the predicted hoop stress at the cladding is larger in this case than in the previous examples.

3- TEXTURE OF THE ZRY CLADDING

The influence of Zry anisotropic mechanical behaviour on the fuel rod performance has been many times neglected in the literature.Notwithstanding the well known dependence of the Zry tube texture and consequently its mechanical response on the fabrication working process,EPRI for example,in its thermal reactor code evaluation project {6} ,recommends the same anisotropy coefficients for claddings with different annealing finishing processes,-heavily cold-worked in case B of Phase III, cold-worked in cases C and D, and fully annealed Zry in case E.

Here the influence of the different cladding annealing temperatures on the fuel performance is studied. The code BACO is used,and Hill's treatment of anisotropic plastic behaviour is adopted. This implies an elliptical yield/creep loci approximation, then the Bauschinger and strength differential effects measured in Zr alloys are not included. In all cases studied the same creep and plasticity laws recommended by EPRI for the Zry cladding are adopted for relating equivalent stresses and strains:

$$\varepsilon_{eq} = f(\sigma_{eq}) \quad ; \quad \dot{\varepsilon}_{eq} = g(\sigma_{eq})$$

where

$$\sigma_{eq} = \left[a_1(\sigma_2-\sigma_3)^2 + a_2(\sigma_3-\sigma_1)^2 + a_3(\sigma_1-\sigma_2)^2\right]^{1/2}$$

then in the different examples the laws for those phenomena differ only in the anisotropy coefficients a_i . Creep and plasticity in a given direction i are taken as

$$\dot{\varepsilon}_i = \frac{g(\sigma_{eq})}{\sigma_{eq}} \left[a_j(\sigma_i-\sigma_k)+a_k(\sigma_i-\sigma_j)\right] \qquad i\neq j\neq k$$

and

$$\varepsilon_i = \frac{f(\sigma_{eq})}{\sigma_{eq}} \left\{ a_j(\sigma_i - \sigma_k) + a_k(\sigma_i - \sigma_j) \right\}_{i \neq j \neq k}$$

The texture and thermal creep resulting from four different annealing treatments were studied by Stehle et al. [13]. In Table IV the annealing conditions of the four Zry specimens and the anisotropy coefficients deduced by those authors are summarized. The four situations range from cold-worked material (Specimen 1) to recrystallized one(Specimen 4). Four different natural uranium fuel rods are then simulated with the same parameters and materials laws usdd in the reference case of Table II except for the cladding,where the previously mentioned anisotropic laws and anisotropy coefficients are used. The same set of coefficients are used for cladding creep and plastic deformation; it must be noted that Stehle et al. fit their anisotropy coefficients to thermal creep loci,but those coefficients may vary for the two phenomena. However,in the examples shown here creep is by large more important than plastic deformation.

The power cycle used for the calculation is composed of:

-Ramp from zero to 250 w/cm in half a day;
-Constant power until 2500 Mw.d/t(U) burnup;
-Ramp from 250 to 550 w/cm in half a day;
-Constant power (550w/cm) until a final burnup of 10000 Mw.d/t(U).

In Figure 2 the calculated permanent displacement(plastic + creep) of the external cladding radius is plotted as a function of burnup. It can be seen that to a larger amount of cold work of the cladding material it corresponds a larger creep down. Durin the power up ramp at 2500 Mw.d/t(U) pellet-clad contact is attaine in the four cases. However,in the examples where a relatively larger creep down of the free cladding is predicted,contact is stablished sooner in the ramp. The predicted hoop stress at the cladding inner surface is plotted in Figure 3 as a function of burnup.There it can be seen that a sharp increase of this stress during the ramp may be expected for the cases where contact is

reached at an early stage -see cases 1 and 2 in the Figure -. However those same cladding materials are able to relax the hoop stress relatively easily. Then after a certain stay in the reactor the predicted hoop stress at the cladding is smaller for the cold-worked material(example 1) and increases with the amount of annealing.

In order to separate the effect of texture from other changes in the material mechanical behaviour,the examples discussed here are based on assuming the creep and plasticity laws for the equivalent stressand strain to be independent of the cladding thermal treatment. If these laws were changed in accordance with the treatment,the relative difference in performance of the different cladding materials should be expected to increase. For example,cold-worked Zry shows a larger creep rate than the annealed one. The same increase in differences of performance should be expected if different anisotropy coefficients were used for irradiation induced creep and growth,being those phenomena more texture dependent than thermal creep.

4- CONCLUSIONS

A set of runs of the BACO code was performed in order to test the sensitivity of the code predicted fuel rod performance on the material models. Several conclusions are drawn. On one side it is shown that relatively minor differences on the fitting of the UO_2 thermal conductivity,well within the scattering among the results of different authors,result in noticeable different numerical predictions. It is important to remark that the difference in predictions is not caused in our examples by the different fitting in the high temperature region,where the uncertainty is larger,but mainly by apparently small differences over the medium and low temperature range.Other parameters,as the roughness constant c in Ross-Stoute gap conductance,elastic modulii and fracture stress,do not seem to have such a large influence on the code predictions.

Finally in section 3 the influence of the Zry cladding

annealing temperature on the fuel performance via differences in texture is studied. Although the model did not include some effect as the strength differential, Bauschinger effect or different anisotropic creep against plastic deformation, it is clearly shown that different textures imply a remarkably different mechanical behaviour of the rod. This implies that fuel mechanical performance is substantially changed by the cladding fabrication thermal treatment not only from the point of material toughness but also by the resulting change in texture.

REFERENCES-

[1] K.Lassmann, Contribution D3/1 to the SMiRT-5 Conference, Berlin, 1979

[2] S.Harriague, G.Coroli and E.J.Savino, Contribution D1/2 to the SMiRT-5 Conference, Berlin, 1979.

[3] S.Harriague, G.Coroli and E.J.Savino, submitted to Nucl.Eng.Des.

[4] M.F.Lyons, GEAP-5100-1, 1965.

[5] R.Brandt and G.Neuer, J.Non-Equil.Thermod. 1, 3, 1976.

[6] H.R.Freeburn, S.R.Pati, I.S.Fiero and M.S.Andrews, EPRI-NP-333, 1977.

[7] MATPRO-09, Tree-NUREG-1005, 1976.

[8] J.A.Christensen, Halden Rep. HIR-84, 1974.

[9] D.E.Scott, WCAP-3269-41, 1965.

[10] J.R.Matthews, AERE-R 2543, 1974.

[11] A.Casario and D.Santinelli, CNEA 13/75/D-CM, 1975.

[12] A.M.Ross and R.L.Stoute, AECL-1552, 1962.

[13] H.Stehle, G.Steinberg and E.Tenckhoff, ASTM-STP 633, p.486, 1977.

[14] Northwood, London and Bahen, J.Nucl.Mater. 55, 299, 1975.

[15] G.Ondracek and B.Schulz, J.Nucl.Mater. 46, 253, 1973.

TABLE I

Fuel rod characteristics

Fuel : natural UO_2

Cladding : Zrly-4

Cold radii :

Pellet external { 0.5294 cm (Table II) / 0.5310 cm (Table III)

Pellet internal 0.0 (compact pellet)

Cladding external 0.595 cm

Cladding internal 0.540 cm

Fuel surface roughness : 0.12×10^{-3} cm

Cladding surface roughness : 0.4×10^{-3} cm

Pellet initial density : 95% TD

External cladding temperature : 305°C (assumed constant)

Coolant pressure : 12 MPa

Fill He pressure at room temperature : 1.7 MPa

Flux depression: included.

TABLE II

Case	End of power up ramp			Final burnup				
	Fuel maxim. temperature (°C)	Surface temper. (°C)		Fuel central temperature (°C)	Surface temper. (°C)		Pellet radius (cm)	Contact pressure (MPa)	Hoop stress clad inner surface(MPa)
		Fuel	Clad		Fuel	Clad			
Reference c=2.5	2273	532	360	2077	417	360	0.54365	35.29	124.5
1- c=1.8	2247	518	360	2051	402	360	0.54292	35.09	118.9
2- c=1.	2224	507	360	2016	394	360	0.54237	34.47	110.4
3-ERR Zry plastic contents [6]	2274	532	360	2074	417	360	0.54332	35.24	123.1
4-ERR UO_2 plastic contents [6]	2290	542	360	2090	417	360	0.54345	35.19	120.4
5-ERR UO_2 fracture stress [6]	2273	532	360	2077	417	360	0.54365	35.34	125.3

TABLE III

	End of power up ramp			Final burnup				
	Fuel centerline temperature (°C)	Surface temper. (°C) Fuel	Clad	Fuel centerline temperature (°C)	Surface temper. (°C) Fuel	Clad	Pellet radius (cm)	Contact pressure (MPa)	Hoop stress clad inner surface (MPa)
Reference case	2182	481	360	2009	416	361	0.54520	35.49	122.9
UO_2 Thermal Conduct.:									
Brandt-Neuer [5]	2079	501	360	1941	417	360	0.54330	33.56	99.3
MATPRO [7]	2051	497	360	1900	417	361	0.54324	33.33	95.3
EPRI [6]	2039	510	360	1877	416	360	0.54325	33.27	93.2
Christensen [8]	2030	500	360	1889	417	360	0.54298	33.05	95.4
Zry Thermal Conduct.									
EPRI [6]	2181	480	358	2022	416	359	0.54506	35.45	121.1

APPENDIX

ALTERNATIVE MATERIAL MODELS USED IN THE CALCULATIONS

1.- Fuel -

1.1 Thermal conductivity (k)

- Reference case: Lyon's correlation 4

$$k=\left(\frac{38.24}{T+129.4}+4.79\times10^{-13}\,T^3\right)\left(1-p\right)^{1.5}$$

using the porosity correction proposed by Ondracek et al. [18] ; T in °K, p is the porosity fraction (assumed constant, p=0.05, in the calculations of section 2), and k in w/cm°K

- Christensen's correlation [8] for 0.95 TD:

$$k=\frac{40.4}{T+191.}+1.32\times10^{-4}\exp(1.88\times10^{-3}(T-273.))$$

for $273°K \leq T \leq 1923°K$

and

$$k=0.02+1.32\times10^{-4}\exp(1.88\times10^{-3}(T-273.))$$

for $1923°K < T < T_{melting}$

- MATPRO's correlation [7] for 95%TD fuel:

$$k=\frac{40.4}{T+191.}+1.216\times10^{-4}\exp(1.867\times10^{-3}(T-273.)) \quad \text{for } T \leq 1923$$

and

$$k=0.0191+1.216\times10^{-4}\exp(1.867\times10^{-3}(T-273.)) \quad \text{for } T > 1923$$

- EPRI's correlation [6] :

$$k=\left(\frac{36.24}{T+129.4}+6.12\times10^{-13}\,T^3\right)\frac{1.1316(1-p^2)}{1+p+10p^2}$$

- Brandt and Neuer correlation [5] :

$$k=\left(\frac{1}{4.39+0.0216\,T}+1.12\times10^{-3}T\exp(-13573/T)-4.18\times10^{3}\exp(-30123/T)\right)$$
$$(1-p(2.74-0.5\times10^{-3}T))$$

1.2 Elastic modulii

- Reference case: Matthews' correlation [10]

$$E=0.22\times10^{6}(1-0.92\times10^{-4}(T-298.))$$
$$\nu=0.3253-1.299\times10^{-4}(T-298.)$$

with E in MPa and T in °K

- EPRI's correlation [6] (+)

$E=0.2025\times10^{6}-97.33\ T$ for $T < 1973$ °K
$E=1.048\times10^{4}$ for $T \geq 1973$ °K

$\nu=0.32-1.791\times10^{-5}(T-298.)$ for $T < 1973$ °K
$\nu=0.29$ for $T \geq 1973$ °K

1.3 Fracture stress

- Reference case: from Matthews [10] an average $\sigma_{fr}=150$ MPa was adopted

- EPRI correlation [6]

$$\sigma_{fr}=108.14+2.186\times10^{-2}T \qquad (\sigma_{fr} \text{ in MPa})$$

2.- Cladding -

2.1 Thermal conductivity (k_{Zry})

- Reference case : from Scott [9] an average value of 0.16 w/cm°K was adopted for in-reactor temperatures.

- MATPRO-9 correlation [7] :

$$k_{Zry}=0.0751+2.09\times10^{-4}T-1.45\times10^{-7}T^{2}+7.67\times10^{-11}T^{3}$$

with k_{Zry} in w/cm°K

2.2 Elastic modulii

Calculations in section 2 were made assuming isotropic behaviour of the cladding.

- Reference case: the following values were determined at CNEN and agree well with those reported by Northwood et al. [14]:

$E=68600$ MPa
$\nu=0.325$

- EPRI correlation:

$E=134970-103.3T$
$\nu=0.3329-0.1265\times10^{-3}T$

(+) This correlation differs markedly either from the one proposed by Matthews [10] or the one in MATPRO [7]. This difference may [illegible] error in reference [6].

3.- Gap conductance -

In the BACO code Ross and Stoute expression [12] for the gap conductance is used:

$$h_g=\frac{\bar{k}\ p_c}{0.5\ R_g\ H}+\frac{k_{fg}}{c(R_1+R_2)+g_1+g_2+d_g}$$

where

h_g = gap conductance (w/cm²°K)

$\bar{k}=\frac{2k_1k_2}{k_1+k_2}$ average thermal conductivity of fuel and cladding (k_1, k_2 thermal conductivities of fuel and cladding)

p_c = contact pressure between fuel and cladding

$R_g=(0.5(R_1^2+R_2^2))^{1/4}$, and R_1, R_2 surface roughnesses offuel and cladding

H = Meyer hardness of the cladding

k_{fg} = thermal conductivity of the gases filling the gap

g_1, g_2 = temperature jump distances

d_g = radial gap

c = constant

In the reference case, constant c is taken equal to 2.5; in section 2 results are compared for values of 1. and 1.8

4.- Zry anisotropy coefficients - [13]

Case	Annealing temperature °C	Anisotropy coefficients F	H	G
1	450	0.52	0.87	0.48
2	500	0.57	0.75	0.43
3	550	0.59	0.51	0.41
4	600	0.65	0.45	0.35

(Annealing time=2.5 h)

with $\sigma_{eq}=\left[F(\sigma_\theta-\sigma_z)^2+H(\sigma_r-\sigma_\theta)^2+G(\sigma_r-\sigma_z)^2\right]^{1/2}$

FIGURE CAPTIONS

Figure 1: UO_2 thermal conductivity for 95% TD vs. temperature. Different fittings to experimental data proposed by:

- Lyons [4]
- EPRI [6]
- MATPRO-09 [7]
- Brandt and Neuer [5]
- Christensen [8]

Figure 2: In site calculated external cladding change of radius due to creep and plastic deformation, for the power cycle summarized in the text, as a function of fuel burn up. Different cases correspond to different anisotropy coefficients for the Zry cladding, described in section 4-Zry anisotropy coefficients- of the Appendix.

Figure 3: Hoop stress at the inner cladding surface as a function of burn up, for the same cases refered to in Figure 2.

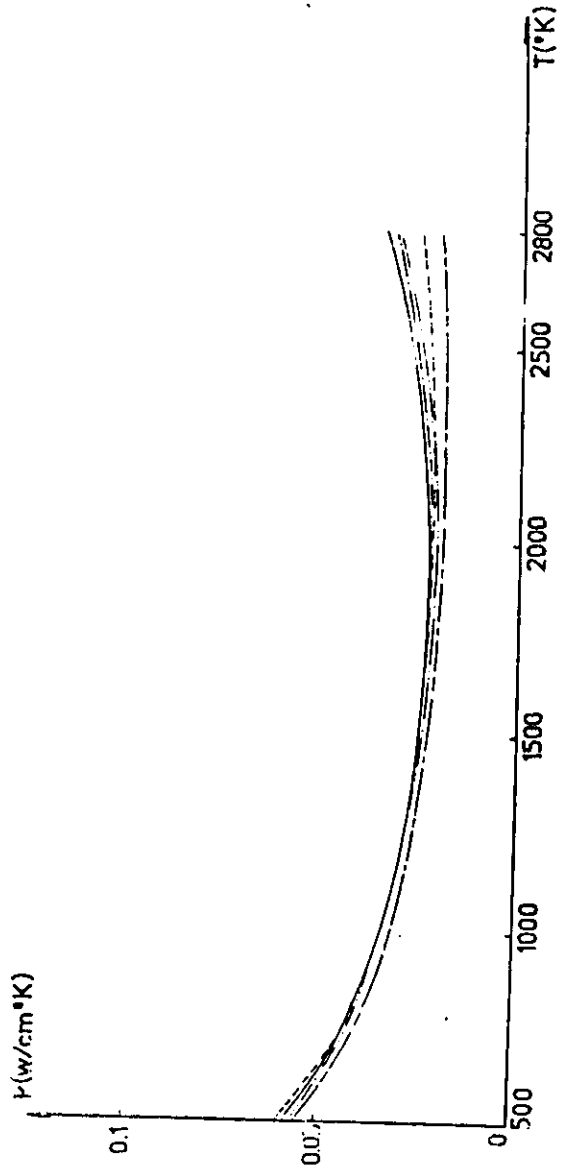

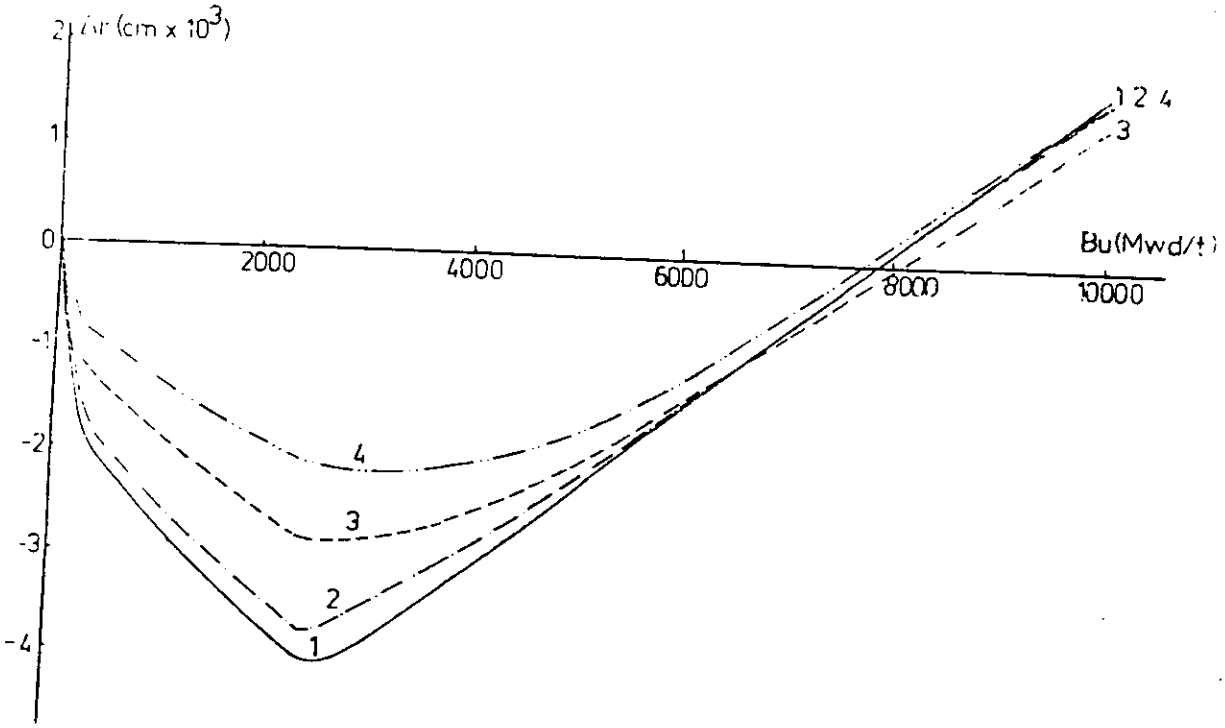
Δr (cm x 10^-3)
2
1
0
-1
-2
-3
-4
2000
4000
6000
8000
10000
Bu(Mwd/t)
1 2 4
3
4
3
2
1

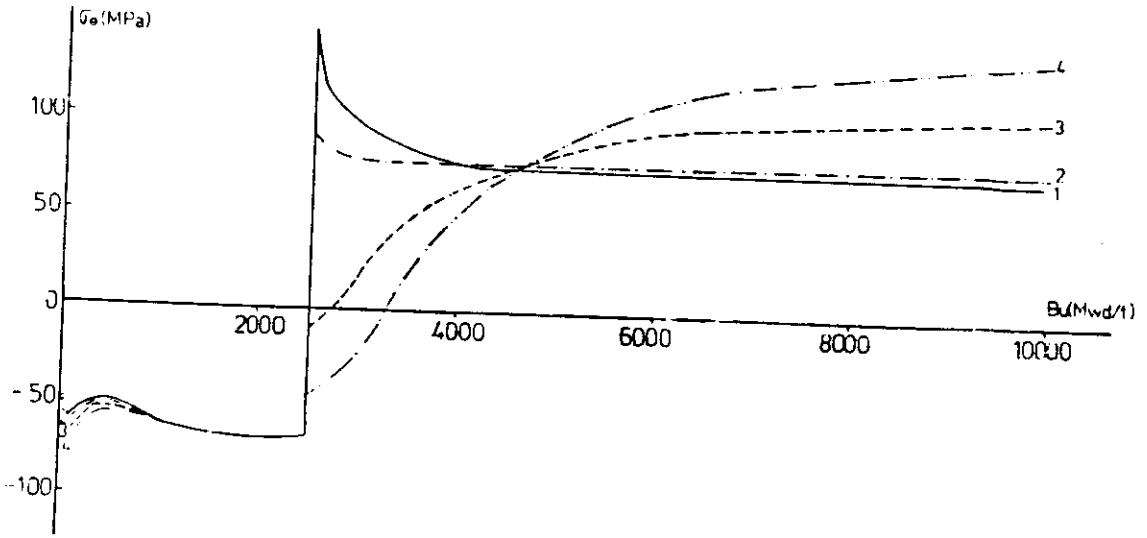
σe(MPa)
100
50
0
-50
-100
2000
4000
6000
8000
10000
Bu(Mwd/t)
4
3
2
1